490 nm with the subtraction of absorbance of background at 650 nm. Furthermore, cell numbers in 6-well plates were also counted after a 24-or 48-h BLM treatment at a dose of 100 μg/ml.

Ligation-mediated polymerase chain reaction (LM-PCR) for the detection of apoptosis-induced nucleosomal ladder

Total genomic DNA was isolated from cells using the Puregene DNA isolation kits from Gentra Systems (Minneapolis, MN). The ApoAlert LM-PCR ladder assay kit from Clontech (Polo Alto, CA) and gel electrophoresis were used to analyze the extent of apoptosis-induced nucleosomal ladder following BLM treatment. LM-PCR was performed according to the manufacturer's instruction. In this study, 500 ng of DNA was used in the ligation reaction to ligate adaptors to the ends of DNA fragments. To further amplify the DNA fragments, 150 ng of ligated DNA was added into the PCR in which the 24-mer adaptor was used as primers and 22 PCR cycles were carried out. The PCR products were electrophoresed in 1.5% agarose gel containing ethidium bromide.

Detection of ROS by dihydrorhodamine 123 (DHR) staining

DHR is an uncharged and nonfluorescent dye that can passively diffuse across membranes. It can be oxidized by ROS to fluorescent and positively charged rhodamine 123, which is preferentially localized in mitochondria [40]. Quantification of ROS levels by the DHR reaction was performed following previous published methods [41,42]. In brief, monolayers of cells grown on glass-bottomed 35-mm dishes (MatTek Corp., Ashland, MA) were prepared. After treatment with BLM, cells were reacted with DHR (Molecular Probes, Eugene, OR) at 37°C for 15 min at a final concentration of 10 μg/ml in a modified Hanks' balanced salt solution (HBSS) containing 10 mM Hepes, 1 mM $MgCl_2$, 2 mM $CaCl_2$, and 2.7 mM glucose and washed with the same buffer twice. Images of rhodamine 123 florescence due to oxidation of DHR were acquired using a CSU-10 confocal laser scanning unit (Yokogawa Electric Co., Tokyo, Japan) coupled to an LX90 inverted microscope (Olympus Optical Co.) and a C5810-01 color chilled 3CCD camera (Hamamatsu Photonics K.K., Japan). Rhodamine 123 from DHR was excited at 488 nm and emission was filtered using a 515-nm barrier filter. Several fields of cells in one dish were scanned randomly and images were recorded. Fluorescent intensity per unit area of each field was quantified using IPLab Spectrum version 3.0 software (Scanalytics Inc., Fairfax, VA). The mean of fluorescent intensity in arbitrary units from several areas in each acquired field was obtained.

SOD activity assay

SOD activity assay was performed according to the method of Spitz and Oberley [43]. Cells were homogenized in 50 mM potassium phosphate buffer (pH 7.8). Total SOD activity was assayed at 25°C by the nitroblue tetrazolium (NBT) reduction assay with bathocuproine sulfonate. The rate of reduction of NBT by superoxide, which was generated from xanthine and xanthine oxidase, was monitored spectrophotometrically at 560 nm. One unit of SOD was defined as the amount of protein which causes a 50% inhibition of the rate of NBT reduction. Sodium cyanide at the concentration of 5 mM was included in the assay mixture to measure MnSOD activity by inhibiting CuZnSOD. CuZnSOD activity was the difference between total SOD activity and MnSOD activity.

CAT activity assay

CAT activity was measured by the method of Beers and Sizer with slight modifications [44]. For both CAT and GPX activity assays, same preparation of samples was used by homogenizing cells in 50 mM phosphate buffer (pH 7.4). Supernatant from 1000*g* centrifugation of cell homogenates was used for assays. The assay reaction for CAT consisted of 50 mM potassium phosphate buffer (pH 7.0), 0.02 M H_2O_2, and samples in a total volume of 1 ml. The reaction was carried out at 25°C. The rate of absorbance change (ΔA/min) at 240 nm was recorded, which indicated the decomposition of H_2O_2. Activities were calculated using the molar extinction coefficient of H_2O_2 at 240 nm, 43.59 L/mol-cm.

GPX activity assay

Activity assays of selenium-dependent GPX were performed as previously described [45,46]. The coupling reagent consisted of 50 mM Tris-Cl buffer (pH 7.7), glutathione, glutathione reductase, sodium cyanide, and NADPH. The coupling reagent in 875 μl and 100 μl of sample was incubated for 2 min at 25°C and hydrogen peroxide (final 25 μM) was added to initiate the reaction. ΔA/min at 340 nm was recorded. ΔA/min of blank, in which sample was replaced by Tris-Cl buffer, was also recorded. The net ΔA/min of samples after subtracting the blank rate was used to calculate the GPX activity using the molar extinction coefficient of NADPH at 340 nm, 6220 L/mol-cm.

Nonradioactive Northern blot analysis

Total RNA was isolated by Trizol (Invitrogen, Carlsbad, CA). The concentration of RNA was determined by measuring the absorbance at 260 nm. Nonradioactive Northern blot analysis to detect steady-state levels of mRNA was performed according to our previous established methods [35]. In brief, 15 μg of total RNA was electrophoresed in 1.5% formaldehyde–agarose gel and transferred to the positive-charged nylon membranes (Roche, USA) in 10X SSC (3 M sodium chloride and 300 mM sodium citrate, pH 7.0 for 20X SSC). Digoxigenin (DIG)-labeled probes for

cDNA fragments of GPX1, GPX4, and MnSOD genes were generated by the PCR DIG probe synthesis kit (Roche) using plasmids containing partial cDNA of those genes as the templates. These plasmids were purified from bacterial clones purchased from Invitrogen except that for MnSOD, which was made in the previous study [39]. Primers for GPX1 were 5′TGACACCCGGCACTTATTAGTGG3′ and 5′GCTTATGACCGACCCCAAGCT3′. Primers for GPX4 were 5′GGCAAGACCGAACTAAACTAC3′ and 5′GTGCACGCTGGATTTTCGG3′. Primers for MnSOD were 5′AGAAGCACAGCCTCCCCGAC3′ and 5′GCAAGCCATGTATCTTTCAGTTA3′. Membranes were prehybridized in hydridization solution (50% deionized formamide, 5X SSC, 0.1% *N*-lauroylsarcosine, 0.02% SDS, 2% blocking reagent from Roche) at 42°C for 1 h and then hybridized with probes in hydridization solution at 42°C overnight. The membrane was then washed twice and detected by the DIG luminescent detection kit (Roche) with alkaline phosphatase-conjugated anti-DIG antibody according to the manufacturer's instruction. Chemiluminescent bands were detected by exposing membranes to the BioMax ML film (Kodak, Rochester, NY). The density of signals on the film from Northern blot analysis and of the 28S rRNA band on the RNA gels photographed by the ChemiDoc system (Biorad, Hercules, CA) was analyzed by the Quantity One Software (Biorad).

Statistical analysis

Data were analyzed by SAS Win 8.1 software (SAS Institute, Cary, NC). One-way analysis of variance (ANOVA) was used to compare the difference among multiple groups. Complete block design was used for data of antioxidant enzyme activities from more than one set of experiments. Data were presented as mean ± standard deviation (SD) except that mean ± standard error of mean (SE) was used for different sets of Northern blot analysis. A level of $P < 0.05$ was considered statistically significant for most experiments except for results of Northern blot analysis in which $P < 0.1$ was considered significant due to the semiquantitative features of Northern blot analysis.

Results

Inhibition of cell growth and Induction of apoptosis by BLM

To compare the effect of 48-h BLM treatment on the cytotoxicity in WI38 and VA13 cells, the amount of viable cells remaining was first accessed by the colorimetric method over a range of doses (10–1000 μg/ml) of BLM and the exact cell number remaining after a 24-or 48-h BLM treatment was counted in both cells at a dose of 100 μg/ml. As shown by Fig. 1, BLM markedly inhibited more growth of viable cells in VA13 cells than in WI38 cells when compared to control groups. The doses that inhibited 50% of

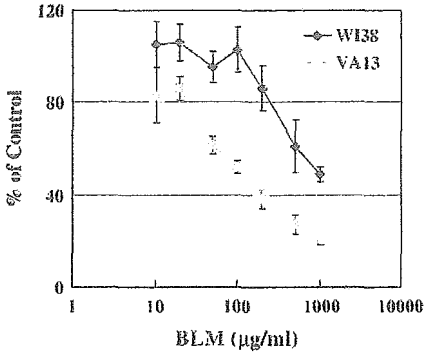

Fig. 1. Growth inhibition assay with a range of BLM doses using the colorimetric method following 48-h treatment. Amount of viable cells was detected by the colorimetric method. Data were represented as percentage of absorbance relative to mean of the control groups ($n = 3$ for each group). The x axis is in log scale.

growth in WI38 and VA13 cells were approximately 120 and 950 μg/ml, respectively. By counting the cell number directly, we confirmed that there were significantly less VA13 cells remaining than WI38 cells following 100 μg/ml of BLM treatment for either 24 or 48 h (Fig. 2). The reduction in cell number was significant in WI38 cells only after a 48-h treatment but not after a 24-h treatment. The extent of reduction was also greater in VA13 cells than in WI38 cells. Most of the cells remaining could not be stained by trypan blue (data not shown). To further evaluate the role of apoptosis in the reduction of cell number after BLM treatment, LM-PCR was performed at different time points. Fig. 3 shows that both WI38 and VA13 cells had the greatest degree of apoptosis-associated nucleosomal fragmentation 24 h after BLM treatment. VA13 cells revealed a higher degree of apoptosis than WI38 cells overall.

Levels of ROS

To measure the production of ROS in cells, DHR was used as the indicator. Cells were treated with 100 μg/ml of CPT for 24 or 48 h and incubated with DHR. As shown in Table 1, there was a significant increase in fluorescent intensity of DHR in WI38 after a 24-h BLM treatment but not in VA13 cells. However, DHR-detectable ROS levels were significantly increased in both WI38 and VA13 cells after a 48-h BLM treatment. On the other hand, the basal level of DHR-detectable ROS was higher in VA13 controls than in WI38 controls. The images of increased fluorescence following 48-h BLM treatment in both cells are demonstrated in Fig. 4.

Activities of primary antioxidant enzymes

Tables 2 and 3 show the activities of primary antioxidant enzymes after 24-and 48-h BLM treatments, respectively. The data were combined from two sets of experiments and analyzed by the complete block design. BLM had no significant effect on the activities of MnSOD, CuZnSOD,

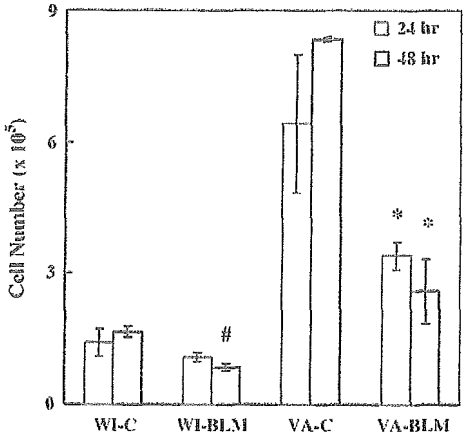

Fig. 2. Percentage of cell number remaining relative to control after 24-and 48-h BLM treatments. Numbers of cells were counted after 24- and 48-h BLM treatments at the dose of 100 μg/mg. Control cells were near confluence at the end of 48-h treatment. Cells remaining in treated groups were all significantly ($P < 0.05$) reduced compared to control groups except that in 24-h treated WI38 groups. WI, WI38 cells; VA, VA13 cells; C, control groups; BLM, BLM-treated groups; # significant difference from WI-C; * significant difference from VA-C.

and CAT. However, BLM increased GPX activities as early as 24 h after BLM treatment and the effect was still significant after a 48-h treatment in VA13 cells. The increase of GPX activity by BLM in WI38 cells was observed only after a 48-h treatment. Moreover, there was no difference in the basal activities of GPX between two cells but those of MnSOD and CAT were significantly lower in VA13 cells compared to WI38 cells.

Steady-state mRNA levels of GPX1, GPX4, and MnSOD

To elucidate whether the increase of GPX activities by BLM was due to up-regulation mRNA levels, we performed nonradioactive Northern blot analysis to detect steady-state

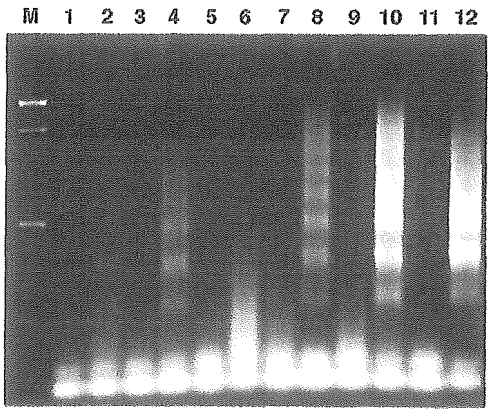

Fig. 3. Ligation-mediated PCR to detect apoptosis-associated DNA fragmentation. DNA was isolated from control cells and cells were treated with 100 μg/mg of BLM for various time points. M, 100-bp ladder; 1, 8-h WI-C; 2, 8-h WI-BLM; 3, 24-h WI-C; 4, 24-h WI-BLM; 5, 48-h WI-C; 6, 48-h WI-BLM; 7, 8-h VA-C; 8, 8-h VA-BLM; 9, 24-h VA-C; 10, 24-h VA-BLM; 11, 48-h VA-C; 12, 48-h VA-BLM.

Table 1
Quantification of intracellular ROS levels detected by DHR

Group	Intensity (arbitrary units)	
	24 h	48 h
WI-control	27.4 ± 1.4 (11)	34.7 ± 1.3 (7)
WI-BLM	31.0 ± 2.1 (10)[a]	41.7 ± 2.5 (7)[a]
VA-control	31.0 ± 2.7 (10)[b]	40.2 ± 2.8 (7)[b]
VA-BLM	32.6 ± 3.0 (10)	55.8 ± 8.5 (6)[c]

Data were presented as mean ± SD (number of replicates).
[a] Significant difference from WI38-control group.
[b] Significant difference from WI38-control group.
[c] Significant difference from VA13-control group.

mRNA levels of GPX1 and GPX4 in cells after BLM treatment (Fig. 5 and Fig. 6). The amount of 28S rRNA visualized on RNA gels was used to normalize the levels of transcripts on films because we have found that the levels of some frequently used housekeeping genes may not exactly match with that of RNA amounts on gels after treatment (data not shown). Fig. 5A and Fig. 5B show the representative results of RNA gels and transcript levels of GPX1 after 24-and 48-h treatments, respectively. The quality of RNA was excellent since the amount of 28S rRNA (upper bands) was much greater than that of 18S rRNA (lower bands). Fig. 5C shows the changes, calculated for three independent experiments, of each group relative to the control of WI38 cells (WI-C) for each time point and their statistical analysis. The results of Fig. 5 demonstrate that the mRNA level of GPX1 was significantly increased in VA13 cells after both a 24-and a 48-h treatment, while it was only increased in WI38 cells after 48 h. We considered $P < 0.1$ as a significant difference because the degrees of the increase in transcript levels could be very variable even though the trend of increase was consistent from experiment to experiment. On the other hand, the basal level of GPX1 between control groups of two cells was not different.

Because MnSOD is highly inducible and, as a mitochondrial matrix protein, its activity could be easily subjected to posttranslational controls by mitochondrial status [47], steady-state mRNA levels of MnSOD after 24-and 48-h BLM treatments were also investigated. Fig. 6 showed the results from one representative experiment examining mRNA levels of GPX4 and MnSOD from the same blot. Statistical analysis from three independent experiments indicated that GPX4 gene expression was not obviously altered by BLM treatment in both cells and was not different between two cells after normalized by the amount of 28S rRNA on gels (data not shown). Moreover, the basal transcript levels of GPX4 were not different between WI38 and VA13 cells. On the other hand, in agreement with the results of activity assays, mRNA levels of MnSOD were much higher in WI38 cells than in VA13 cells for both 1-and 4-kb transcripts, but not changed to a considerable amount after BLM treatment from two sets of experiments. The levels of the 1-kb transcript in the control of VA13 cells shown by Fig. 6 were about 60 and 50% of that in the

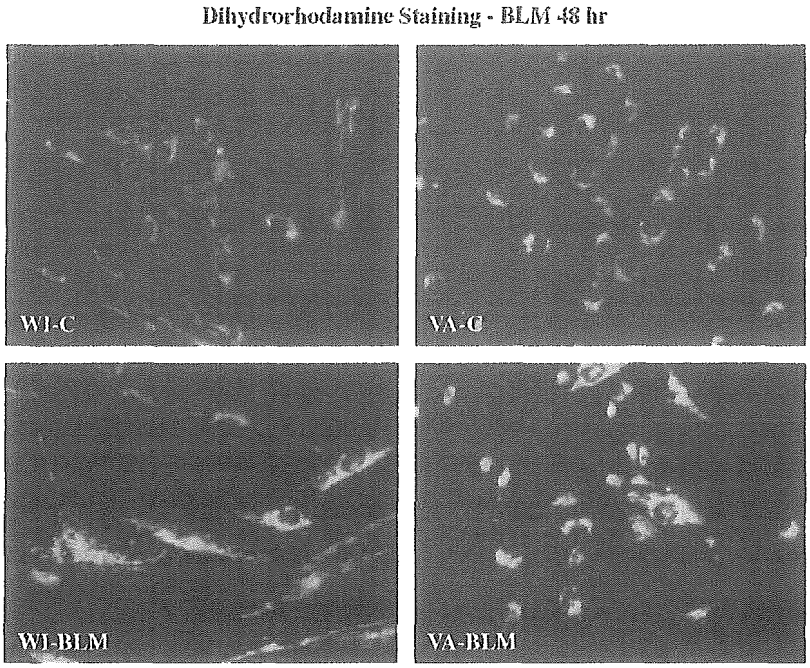

Fig. 4. Intracellular ROS detected by DHR after 48-h BLM treatment. The fluorescence intensity was significantly increased after BLM treatment in both cells.

control of WI38 cells for the 24-and 48-h treatment groups, respectively. However, the basal levels of the 4-kb transcript in VA cells were about 40 and 30% of those in WI38 cells for the 24-and 48-h treatment groups, respectively.

Discussion

As an anticancer drug, BLM unsurprisingly caused a higher degree of growth inhibition and apoptosis in VA13 cells than normal WI38 cells. However, BLM induced oxidative stress earlier in WI38 cells than in VA13 cells as demonstrated by an earlier increase of DHR-detectable intracellular ROS levels and later induction of GPX1 in WI38 cells, which may not be directly linked to the DNA-damaging effect of BLM. Therefore, when normal WI38 cells became transformed, it presented a different status of oxidative stress in response to BLM.

No previous study demonstrated generation of intracellular ROS from BLM in live cultured cells or in animal tissues. DHR is a diffusible compound that is able to detect ROS such as hydrogen peroxide in the presence of peroxidases, hydroxyl radicals, and peroxynitrite, but not superoxide radicals [48,49]. Because oxidized DHR, rhodamine 123, is detected in the mitochondria, increased DHR oxidation may indicate ROS generation in mitochondria or in the compartments close to mitochondria. By using this method, we showed that BLM could increase intracellular ROS levels after both 24-and 48-h treatments in WI38 cells but only after a 48-h treatment in VA13 cells. However, we could not identify which species of ROS were generated.

The earlier increase of GPX activities in VA13 cells after BLM treatment could contribute to a lesser increase in DHR-detectable ROS levels in VA13 cells, which could be a response to BLM-generated oxidative stress but may not compensate for increased oxidative stress. However, the growth inhibitory effect of BLM was much greater to VA13 cells than to WI38 cells, which could result from preferential effects of DNA strand breaks and chromosomal aberrations induced by BLM [9] in fast-proliferating tumor cells. It is possible that formation of nuclear ROS is not readily detected by DHR or ROS formation was not the only

Table 2
Activities of primary antioxidant enzymes after 24-h BLM treatment

	CuZnSOD (units/mg)	MnSOD (units/mg)	CAT (μmol/min/mg)	GPX (nmol/min/mg)
WI-control	21.7 ± 5.0 (5)	30.7 ± 5.3 (5)	10.8 ± 2.8 (7)	18.1 ± 2.5 (6)
WI-BLM	23.5 ± 1.8 (4)	28.8 ± 6.7 (4)	10.0 ± 1.9 (7)	16.7 ± 2.4 (6)
VA-control	19.2 ± 2.0 (5)	5.0 ± 1.9 (5)[a]	6.6 ± 1.1 (6)[a]	21.2 ± 5.1 (6)
VA-BLM	19.6 ± 5.8 (4)	4.8 ± 0.5 (4)[a]	6.8 ± 1.4 (6)[a]	27.7 ± 4.1 (6)[b]

Data were presented as mean ± SD (number of replicates).
[a] Significant difference from WI38-control or WI38-BLM group.
[b] Significant difference from VA13-control group.

Table 3
Activities of primary antioxidant enzymes after 48-h BLM treatment

	CuZnSOD (units/mg)	MnSOD (units/mg)	CAT (μmol/min/mg)	GPX (nmol/min/mg)
WI-control	18.4 ± 8.6 (5)	21.9 ± 13.0 (5)	10.6 ± 2.4 (6)	21.8 ± 5.2 (6)
WI-BLM	20.5 ± 7.2 (5)	29.4 ± 12.2 (5)	9.9 ± 0.7 (6)	37.5 ± 14.0 (6)[a]
VA-control	17.2 ± 2.0 (5)	4.2 ± 1.4 (5)[b]	7.8 ± 1.4 (6)[b]	20.7 ± 2.2 (6)
VA-BLM	17.8 ± 3.8 (5)	4.4 ± 1.3 (5)[b]	5.9 ± 0.9 (6)[b]	31.1 ± 3.5 (6)[c]

Data were presented as mean ± SD (number of replicates).
[a] Significant difference from WI38-control group.
[b] Significant difference from WI38-control or WI38-BLM group.
[c] Significant difference from VA13-control group.

determinant in DNA damage following BLM treatment since some researchers proposed that BLM-induced strand break and base propenal formation could be independent from ROS [1,13]. It is also possible that lower basal activities of MnSOD and CAT in VA13 cells made VA13 cells more susceptible to oxidative damage and apoptosis by BLM. Moreover, ROS undetectable by DHR, such as superoxide, could be involved as MnSOD was able to protect cells against oxidative stress-associated apoptosis [41,50]. Nevertheless, earlier oxidative stress in WI38 cells would result in the interruption of normal cellular function, although there may be no immediate effect on growth. Furthermore, generation of ROS or oxidative damage induced by BLM in intact cells was not necessarily confined in the nuclei and therefore its possible adverse effects on other cellular compartments, such as mitochondria, and other macromolecules, such as lipid and protein, would have great implications in BLM-induced toxicity, which has not been well studied in the literature.

We have found that *N*-acetyl-L-cysteine (NAC) at 1 mM, which could completely protect VA13 cells against cytotoxicity induced by a 48-h treatment of hydrogen peroxide (100 μM) when treated together with hydrogen peroxide, was unable to exert any protective effect against BLM (500 μg/ml)-induced cytotoxicity in either WI38 or VA13 cells using the colorimetric assay either by pretreating cells with NAC before BLM treatment or by treating cells with NAC at the same time as BLM treatment (data not shown). NAC has been widely used an antioxidant that can both enhance intracellular GSH [51] and directly scavenge some species of ROS, especially hydroxyl radicals [52–54]. It has been

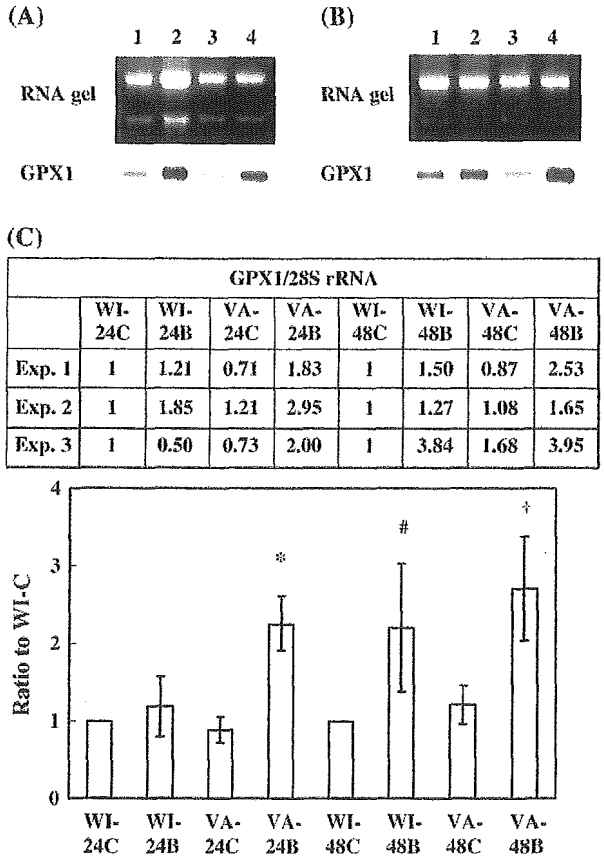

Fig. 5. Results of Northern blot analysis for the detection of GPX1 RNA levels following BLM treatment. (A) The RNA gel and transcript levels of GPX1 from cells treated for 24 h. (B) The RNA gel and transcript levels of GPX1 from cells treated for 48 h. (C) The density of GPX1 gene on the film was normalized by that of 28S rRNA bands on RNA gels. The relative changes to the control of WI38 cells for each time point from three sets of experiments are presented in the upper table. Data in mean ± SE values calculated from three independent experiments are then presented in the lower graph. Upper and lower bands of RNA gels in (A) and (B) indicate 28S rRNA and 18S rRNA, respectively. 1, WI-C; 2, WI-BLM, 3, VA-C; 4, VA-BLM; C, control; B, BLM; $^{*}P < 0.01$ vs VA-C or WI-BLM; $^{\#}P < 0.1$ vs WI-C; $^{\dagger}P < 0.05$ vs VA-C.

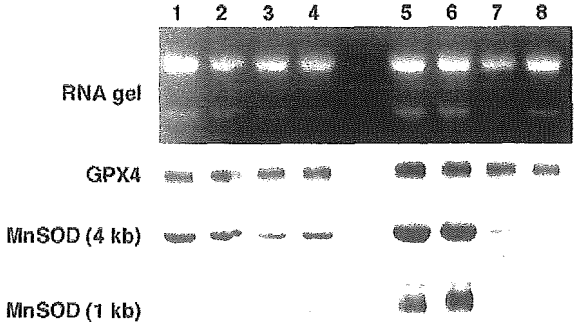

Fig. 6. Northern blot analysis for detecting RNA levels of GPX4 and MnSOD after 24-and 48-h BLM treatments. Groups 1 to 4 belong to the 24-h treatment groups. Groups 5 to 8 groups belong to the 48-h treatment groups. 1 and 5, WI-C; 2 and 6, WI-BLM; 3 and 7, VA-C; 4 and 8, VA-BLM.

indicated that NAC can react with hydrogen peroxide but its slow reaction with superoxide is not considered physiologically significant [52–54]. Moreover, unlike cisplatin [51], depletion of GSH as a target in BLM-induced cytotoxicity has not been indicated previously and it has been shown that reduction of ferric BLM complex to Fe(II)-BLM complex by glutathione or superoxide is important for forming activated BLM to damage DNA in vitro [2]. Chattopadhyay et al. showed that the clastogenic activity of BLM on normal lymphocytes was reduced after GSH depletion and enhanced after GSH addition [55]. Our results that NAC had no effect on cytotoxicity of both cells indicate that either GSH from NAC or NAC itself was not the appropriate antioxidant against BLM-induced oxidative stress or antioxidant effects of NAC outside the nucleus was compromised by the ROS-independent DNA damage promoted by GSH after BLM treatment. On the other hand, whether increased GSH or NAC in cytosol could also enhance their amount in mitochondria was also uncertain as a specific carrier is required for the transport of GSH into mitochondria [56] if mitochondrion is a source of oxidative stress in BLM-induced toxicity.

It has been hypothesized by Oberley that a lower MnSOD level is a characteristic of tumor cells [34] and reversion of transformed phenotypes by overexpression of MnSOD could be due to increased levels of hydrogen peroxide [57]. However, it has also been shown that elevated MnSOD levels in cultured tumor cells reduced oxidative stress in other studies without increased basal levels of hydrogen peroxide [41,50]. In the current study, we showed that markedly lower MnSOD and CAT activities in VA13 cells in fact were associated with higher DHR-detectable ROS levels. Lower MnSOD activities and higher GSH levels in VA13 cells [37] may actually promote formation of damaging glutathionyl radicals ($GS^{\cdot}$) in the mitochondria [53]. Moreover, antioxidant enzymes may play different roles in normal versus tumor cells via mechanisms independent of hydrogen peroxide. For example, overexpression of MnSOD in transgenic mice could protect hearts against toxicity induced by adriamycin [58,59], which generates superoxide, but reduced radiation control dose in fibrosarcoma cells when grown in mice [60]. On the other hand, it has been shown that human MnSOD has two major transcripts in the length of about 1 and 4 kb [61]. Our study not only confirmed lower MnSOD activities in VA13 cells that have been previously reported [36], but also first showed that both transcripts of MnSOD were higher in WI38 cells than in VA13 cells. Levels of 4-kb transcripts were much higher than that of 1-kb transcripts in both cells. Although whether the 4-kb transcript is functional has never been studied, it is very possible that the 4-kb transcript also contributes to the difference in MnSOD activities observed. In addition to lower MnSOD activities, we also found that activities of CAT were lower in VA13 cells, but activities of CuZnSOD and GPX were unchanged.

Our study is the first to demonstrate induction of GPX1 transcripts along with the increase of GPX activity by BLM. Previous studies studying BLM and antioxidant enzymes did not investigate transcript levels. Some studies detecting GPX mRNA levels also did not specify which form of GPX gene was detected [23,24]. It has been shown that the 5′-flanking region of the human GPX1 gene contains AP-1-binding sites and oxygen-responsive elements (ORE), which could contribute to the regulation of this gene by phorbol ester, oxygen tension, and xenobiotics [22,62,63]. It has also been found that the increase of nitric oxide level caused inactivation of GPX but induction of GPX gene expression [24] and ozone increased both activities and RNA levels of GPX in rat lungs [64]. Therefore, GPX is not necessarily only specifically induced by hydrogen peroxide but can respond to altered redox status modulated by different conditions. Results from this study suggest that GPX1 gene induction was responsible for increased GPX activities following BLM treatment in both cells. However, the increase of GPX activities in WI38 cells occurred later than the increase of ROS levels and GPX1 induction preceded ROS increase in VA13 cells, indicating differential regulation of GPX1 by BLM in these two cells. The differential responses of GPX1 in WI38 and VA13 cells to BLM could be due to altered redox regulation of gene expression or signal transduction following transformation. It is possible that molecules other than DHR-detectable ROS but related to oxidative stress following BLM treatment induced GPX1. Alternatively, GPX1 in VA13 cells was more easily induced by smaller increase of ROS that became insignificant compared to higher basal levels of ROS in VA13 cells. Furthermore, since the majority of GPX1 should be present in the cytosol, increased GPX1 may not compensate for oxidative stress in mitochondria completely. On the other hand, we did not observe any change in the activities of MnSOD, CuZnSOD, and CAT following BLM treatment. It has been shown that those antioxidant enzymes responded to the same sources of ROS in a different manner. For example, Shull et al. showed that hydrogen peroxide treatment resulted in more GPX and CAT transcript levels but not CuZnSOD levels in the tracheal epithelial cell line, while superoxide generated extracellularly from the xanthione/xanthione oxidase system induced only MnSOD mRNA levels but not that of GPX, CAT, and CuZnSOD [23]. Since other primary antioxidant enzymes were not altered by BLM treatment in our study, why GPX1 was selectively induced and its role in BLM-induced cytotoxicity or possibly BLM resistance remain to be investigated.

In conclusion, our results indicate that BLM caused oxidative stress at an earlier time point in WI38 cells, although it induced higher cytotoxicity in VA13 cells. The use of normal or tumor cells in studying oxidative stress and toxicity induced by BLM may therefore have distinct implications. In addition to differential responses between WI38 and VA13 cells to BLM, the role of selective GPX1 induction by BLM also has implications in understanding

chemotherapy using BLM and cellular or molecular events not directly related to the interaction of BLM with nuclear DNA.

Acknowledgments

This work was supported by Grants NSC 89-2314-B-182-070 and NSC 90-2320-B-182-061 from National Science Council, Taiwan. We thank Dr. Daret K. St. Clair at the University of Kentucky for helpful discussion.

References

[1] Hay, J.; Shahzeidi, S.; Laurent, G. Mechanisms of bleomycin-induced lung damage. *Arch. Toxicol.* **65:**81–94; 1991.

[2] Sugiura, Y.; Suzuki, T.; Kuwahara, J.; Tanaka, H. On the mechanism of hydrogen peroxide-, superoxide-, and ultraviolet light-induced DNA cleavages of inactive bleomycin-iron (III) complex. *Biochem. Biophys. Res. Commun.* **105:**1151–1158; 1982.

[3] Oberley, L. W.; Buettner, G. R. The production of hydroxyl radical by bleomycin and iron (II). *FEBS Lett.* **97:**47–49; 1979.

[4] Buettner, G. R.; Moseley, P. L. Ascorbate both activates and inactivates bleomycin by free radical generation. *Biochemistry* **21:**9784–9978; 1992.

[5] Mahmutoglu, I.; Scheulen, M. E.; Kappus, H. Oxygen radical formation and DNA damage due to enzymatic reduction of bleomycin-Fe(III). *Arch. Toxicol.* **60:**150–153; 1987.

[6] Kanofsky, J. R. Singlet oxygen production by bleomycin. *J. Biol. Chem.* **261:**13546–13550; 1986.

[7] Gutteridge, J. M. C.; West, M.; Eneff, K.; Floyd, R. A. Bleomycin-iron damage to DNA with formation of 8-hydroxydeoxyguanosine and base propenals. Indication that xanthine oxidase generates superoxide from DNA degradation products. *Free Radic. Res. Commun.* **10:**159–165; 1990.

[8] Turner, M. J.; Bozarth, C. H.; Strauss, K. E. Evidence for intracellular superoxide formation following the exposure of guinea pig erythrocytes to bleomycin. *Biochem. Pharmacol.* **38:**85–90; 1999.

[9] Benitez-Bribiesca, L.; Sanchez-Suarez, P. Oxidative damage, bleomycin, and gamma radiation induce different types of DNA strand breaks in normal lymphocytes and thymocytes. *Ann. N.Y. Acad. Sci.* **887:**133–149; 1999.

[10] Giri, S. N.; Chen, Z. L.; Younker, W. R.; Schiedt, M. J. Effects of intratracheal administration of bleomycin on GSH-shuttle enzymes, catalase, lipid peroxidation, and collagen content in the lungs of hamster. *Toxicol. Appl. Pharmacol.* **71:**132–141; 1983.

[11] Khadir, A.; Verreault, J.; Averill, D. A. Inhibition of antioxidants and hyperthermia enhance bleomycin-induced cytotoxicity and lipid peroxidation in Chinese hamster ovary cells. *Arch. Biochem. Biophys.* **370:**163–175; 1999.

[12] Roberts, L. J. II; Morrow, J. D. Measurement of F2-isoprostanes as an index of oxidative stress in vivo. *Free Radic. Biol. Med.* **28:**505–513; 2000.

[13] Gajewski, E.; Aruoma, O. I.; Dizdaroglu, M.; Halliwell, B. Bleomycin-dependent damage to the bases in DNA is a minor side reaction. *Biochemistry* **30:**2444–2448; 1991.

[14] Halliwell, B.; Gutteridge, J. M. C. *Free radicals in biology and medicine*. New York: Oxford University Press; 1999.

[15] Zelko, I. N.; Mariani, T. J.; Folz, R. J. Superoxide dismutase multigene family: a comparison of the CuZn-SOD (SOD1), Mn-SOD (SOD2), and EC-SOD (SOD3) gene structures, evolution, and expression. *Free Radic. Biol. Med.* **33:**337–349; 2002.

[16] Imai, H.; Nakagawa, Y. Biological significance of phospholipid hydroperoxide glutathione peroxidase (PHGPx, GPx4) in mammalian cells. *Free Radic. Biol. Med.* **34:**145–169; 2003.

[17] Esposito, L. A.; Kokoszka, J. E.; Waymire, K. G.; Cottrell, B.; MacGregor, G. R.; Wallace, D. C. Mitochondrial oxidative stress in mice lacking the glutathione peroxidase-1 gene. *Free Radic. Biol. Med.* **28:**754–766; 2000.

[18] Akashi, M.; Hachiya, M.; Paquette, R. L.; Osawa, Y.; Shimizu, S.; Suzuki, G. Irradiation increases manganese superoxide dismutase mRNA levels in human fibroblasts. *J. Biol. Chem.* **270:** 15864–15869; 1995.

[19] Wong, G. H. W.; Goeddel, D. V. Induction of manganous superoxide dismutase by tumor necrosis factor: possible protective mechanism. *Science* **241:**941–944; 1988.

[20] Crosby, A.; Wahle, K. W. J.; Duthie, G. G. Modulation of glutathione peroxidase activity in human vascular endothelial cells by fatty acids and the cytokine interleukin-1β. *Biochim. Biophys. Acta* **1303:**187–192; 1996.

[21] Quinlan, T.; Spivack, S.; Mossman, B. T. Regulation of antioxidant enzymes in lung after oxidant injury. *Environ. Health Perspect.* **102 (Suppl. 2):**79–87; 1994.

[22] Jornot, L.; Junod, A. F. Hyperoxia, unlike phorbol ester, induces glutathione peroxidase through a protein kinase C-independent mechanism. *Biochem. J.* **326:**117–123; 1997.

[23] Shull, S.; Heintz, N. H.; Periasamy, M.; Manohar, M.; Janssen, Y. M. W.; Marsh, J. P.; Mossman, B. T. Differential regulation of antioxidant enzymes in response to oxidants. *J. Biol. Chem.* **266:**24398–24403; 1991.

[24] Dobashi, K.; Asayama, K.; Nakane, T.; Kodera, K.; Hayashibe, H.; Nakazawa, S. Induction of glutathione peroxidase in response to inactivation by nitric oxide. *Free Radic. Res.* **35:**319–327; 2001.

[25] Dalton, T. P.; Puga, A. Regulation of gene expression by reactive oxygen. *Annu. Rev. Pharmacol. Toxicol.* **39:**67–101; 1999.

[26] Xu, Y.; Kiningham, K. K.; Devalaraja, M. N.; Yeh, C. C.; Majima, H.; Kasarskis, E. J.; St.Clair, D. K. An intronic NF-kappaB element is essential for induction of the human manganese superoxide dismutase gene by tumor necrosis factor-α and interleukin-1β. *DNA Cell Biol.* **18:**709–722; 1999.

[27] Phan, S. H.; Fantone, J. C. Inhibition of bleomycin-induced pulmonary fibrosis by lipopolysaccharide. *Lab. Invest.* **50:**587–591; 1984.

[28] Filderman, A. E.; Genovese, L. A.; Lazo, J. S. Alterations in pulmonary protective enzymes following systemic bleomycin treatment in mice. *Biochem. Pharmacol.* **37:**1111–1116; 1988.

[29] Fantone, J. C.; Phan, S. H. Oxygen metabolite detoxifying enzyme levels in bleomycin-induced fibrotic lungs. *Free Radic. Biol. Med.* **4:**388–402; 1988.

[30] Hiraiwa, K.; Oka, T.; Yagi, K. Effect of bleomycin on lipid peroxides, glutathione peroxidase and collagenase in cultured lung fibroblasts. *J. Biochem.* **93:**1203–1210; 1983.

[31] Allen, R. G.; Balin, A. K. Effects of oxygen on the antioxidant responses of normal and transformed cells. *Exp. Cell Res.* **289:** 307–316; 2003.

[32] Hileman, E. O.; Liu, J.; Albitar, M.; Keating, M. J.; Huang, P. Intrinsic oxidative stress in cancer cells: a biochemical basis for therapeutic selectivity. *Cancer Chemother. Pharmacol.* **53:**209–219; 2004.

[33] Bize, I. B.; Oberley, L. W.; Morris, H. P. Superoxide dismutase and superoxide radical in Morri Hepatomas. *Cancer Res.* **40:**3369–3686; 1980.

[34] Oberley, L. W.; Oberley, T. D. Role of antioxidant enzymes in cell immortalization and transformation. *Mol. Cell. Biol.* **84:**147–153; 1988.

[35] Yen, H.-C.; Nien, C.-Y.; Majima, H.J.; Lee, C.-P.; Chen, S.-Y.; Wei, J.-S.; See, L.-C. Increase of lipid peroxidation by cisplatin in WI38 cells but not in SV40-transformed WI38 cells. *J. Biochem. Mol. Toxicol.* **17:**39–46; 2003.

[36] Oberley, L. W.; McCormick, M. L.; Sierra-Rivera, E.; St.Clair, D. K. Manganese superoxide dismutase in normal and transformed human embryonic lung fibroblasts. *Free Radic. Biol. Med.* **6**:379–384; 1989.

[37] Wan, X. S.; St.Clair, D. K. Differential cytotoxicity of buthionine sulfoximine to "normal" and transformed human lung fibroblast cells. *Cancer Chemother. Pharmacol.* **33**:210–214; 1993.

[38] Chabot, B.; Frappier, D.; Branche, H. L. Differential ASF/SF2 activity in extracts from normal WI38 and transformed WI38VA13 cells. *Nucleic Acids Res.* **20**:5197–5204; 1992.

[39] Chen, Z. P.; Schell, J. B.; Ho, C.-T.; Chen, K. Y. Green tea epigallocatechin gallate shows a pronounce growth inhibitory effect on cancerous cells but not on their normal counterparts. *Cancer Lett.* **129**:173–179; 1998.

[40] Haugland, R. P. *Handbook of fluorescent probes and research products*. Web edition. Eugene: Molecular Probes; 2002.

[41] Motoori, S.; Majima, H. J.; Ebara, M.; Kato, H.; Hirai, F.; Kakinuma, S.; Yamaguchi, C.; Ozawa, T.; Nagano, T.; Tsujii, H.; Saisho, H. Overexpression of mitochondrial manganese superoxide dismutase protects against radiation-induced cell death in the human hepatocellular carcinoma cell line HLE. *Cancer Res.* **61**:5382–5388; 2001.

[42] Hirai, F.; Motoori, S.; Kakinuma, S.; Tomita, K.; Indo, H. P.; Yamaguchi, T.; Yen, H.-C.; St.Clair, D. K.; Nagano, T.; Ozawa, T.; Saisho, H.; Majima, H. J. Mitochondrial signal lacking manganese superoxide dismutase failed to prevent cell death by reoxygenation following hypoxia in a human pancreatic cancer cell line, KP4. *Antioxid. Redox Sign.* **6**:523–535; 2004.

[43] Spitz, D. R.; Oberley, L. W. An assay for superoxide dismutase activity in mammalian tissue homogenates. *Anal. Biochem.* **179**:8–18; 1989.

[44] Beers, R. F.; Sizer, I. W. A spectrophotometric method for measuring the breakdown of hydrogen peroxide by catalase. *J. Biol. Chem.* **195**:133–140; 1952.

[45] St. Clair, D. K.; Chow, C. K. Glutathione peroxidase: activity and steady-state level of mRNA. In: Punchard, N. A., Kelly, F. J., eds. *Free radicals. A practical approach*. New York: Oxford University Press; 1996: pp. 227–240.

[46] Yen, H.-C.; Chen, B.-S.; Hsu, Y.-T. Effect of anticoagulants and storage of coupling reagent on the activity assay of extracellular glutathione peroxidase in human plasma. *J. Biomed. Lab. Sci.* **16**:6–10; 2004.

[47] Pfanner, N.; Wiedemann, N. Mitochondrial protein import: two membranes, three translocases. *Curr. Opin. Cell Biol.* **14**:400–411; 2002.

[48] Royall, J. M.; Ischiropoulos, H. Evaluation of 2′-7′-dichlorofluorescin and dihydrorhodamine 123 as fluorescent probes for intracellular H_2O_2 in cultured endothelial cells. *Arch. Biochem. Biophys.* **302**:348–355; 1993.

[49] Kooy, N. W.; Royall, J. M.; Ischiropoulos, H.; Beckman, J. S. Peroxynitrite-mediated oxidation of dihydrorhodamine 123. *Free Radic. Biol. Med.* **16**:149–156; 1994.

[50] Majima, H. J.; Oberley, T. D.; Furukawa, K.; Mattson, M. P.; Yen, H.-C.; Szweda, L. I.; St.Clair, D. K. Prevention of mitochondrial injury by manganese superoxide dismutase reveals a primary mechanism for alkaline-induced cell death. *J. Biol. Chem.* **273**:8217–8224; 1998.

[51] Salahudeen, A.; Poovala, V.; Parry, W.; Pande, R.; Kanji, V.; Ansari, N.; Morrow, J.; Roberts, J., II. Cisplatin induces N-acetyl cysteine suppressible F_2-isoprostane production and injury in renal tubular epithelial cells. *J. Am. Soc. Nephrol.* **9**:1445–1448; 1998.

[52] Winterbourn, C. C.; Metodiwa, D. Reactivity of biologically important thiol compounds with superoxide and hydrogen peroxide. *Free Radic. Biol. Med.* **27**:322–328; 1999.

[53] Jones, C. M.; Lawrence, A.; Wardman, P.; Burkitt, M. J. Kinetics of superoxide scavenging by glutathione: an evaluation of its role in the removal of mitochondrial superoxide. *Biochem. Soc. Trans.* **31**: 1337–1339; 2003.

[54] Aruoma, O. I.; Halliwell, B.; Hoey, B. M.; Butler, J. The antioxidant action of N-acetylcysteine: its reaction with hydrogen peroxide, hydroxyl radical, superoxide, and hypochlorus acid. *Free Radic. Biol. Med.* **6**:593–597; 1989.

[55] Chattopadhyay, A.; Choudhury, S.; Chatterjee, A. Modulation of clastogenic activity of bleomycin by reduced-glutathione, glutathione-ester and buthionine sulfoximine. *Mutagenesis* **12**:221–225; 1997.

[56] Fernandez-Checa, J. C.; Kaplowitz, N.; Garcia-Ruiz, C.; Colell, A.; Miranda, M.; Mari, M.; Ardite, E.; Morales, A. GSH transport in mitochondria: defense against TNF-induced oxidative stress and alcohol-induced defect. *Am. J. Physiol.* **273**:G7–G17; 1997.

[57] Zhong, W.; Oberley, L. W.; Oberley, T. D.; Yan, T.; Domann, F. E.; St.Clair, D. K. Inhibition of cell growth and sensitization to oxidative damage by overexpression of manganese superoxide dismutase in rat glioma cells. *Cell Growth Differ.* **7**:1175–1186; 1996.

[58] Yen, H.-C.; Oberley, T. D.; Vichitbandha, S.; Ho, Y.-S.; St.Clair, D. K. The protective role of manganese superoxide dismutase against adriamycin-induced acute cardiac toxicity in transgenic mice. *J. Clin. Invest.* **98**:1253–1260; 1996.

[59] Yen, H.-C.; Oberley, T. D.; Gairola, C. G.; Szweda, L. I.; St.Clair, D. K. Manganese superoxide dismutase protects mitochondrial complex I against adriamycin-induced cardiomyopathy in transgenic mice. *Arch. Biochem. Biophys.* **362**:59–66; 1999.

[60] Urano, M.; Kuroda, M.; Reynolds, R.; Oberley, T. D.; St.Clair, D. K. Expression of manganese superoxide dismutase reduced tumor control radiation dose: gene-radiotherapy. *Cancer Res.* **55**:2490–2493; 1995.

[61] Wispe, J. R.; Clark, J. C.; Burhans, M. S.; Kropp, K. E.; Korfhagen, T. R.; Whitsett, J. A. Synthesis and processing of the precursor for human mangano-superoxide dismutase. *Biochim. Biophys. Acta* **994**:30–36; 1989.

[62] Cowan, D. B.; Weisel, R. D.; Williams, W. G.; Mickle, D. A. G. Identification of oxygen responsive elements in the 5-flanking region of the human glutathione peroxidase gene. *J. Biol. Chem.* **268**: 26904–26910; 1993.

[63] Moscow, J. A.; Morrow, C. S.; He, R.; Mullenbach, G. T.; Cowan, K. H. Structure and function of the 5-flanking sequence of the human cytosolic selenium-dependent glutathione peroxidase gene (hgpx1). *J. Biol. Chem.* **267**:5949–5958; 1992.

[64] Rahman, I.; Clearch, L. B.; Massaro, D. Rat lung antioxidant enzyme induction by ozone. *Am. J. Physiol.* **260**:L412–L418; 1991.

Increased expression of humanin peptide in diffuse-type pigmented villonodular synovitis: implication of its mitochondrial abnormality

K Ijiri, H Tsuruga, H Sakakima, K Tomita, N Taniguchi, K Shimoonoda, S Komiya, M B Goldring, H J Majima and T Matsuyama

Ann. Rheum. Dis 2005;64;816-823; originally published online 26 Nov 2004; doi:10.1136/ard.2004.025445

EXTENDED REPORT

Increased expression of humanin peptide in diffuse-type pigmented villonodular synovitis: implication of its mitochondrial abnormality

K Ijiri, H Tsuruga, H Sakakima, K Tomita, N Taniguchi, K Shimoonoda, S Komiya, M B Goldring, H J Majima, T Matsuyama

Ann Rheum Dis 2005;64:816–823. doi: 10.1136/ard.2004.025445

See end of article for authors' affiliations

Correspondence to: Dr K Ijiri, Beth Israel Deaconess Medical Center, Harvard Institutes of Medicine, Room 237, 4 Blackfan, Circle, Boston, MA 02115, USA; kijiri@bidmc.harvard.edu

Accepted 27 October 2004
Published Online First 26 November 2004

Objectives: To define the pathogenesis of pigmented villonodular synovitis (PVNS), by searching for highly expressed genes in primary synovial cells from patients with PVNS.
Methods: A combination of subtraction cloning and Southern colony hybridisation was used to detect highly expressed genes in PVNS in comparison with rheumatoid synovial cells. Northern hybridisation was performed to confirm the differential expression of the humanin gene in PVNS. Expression of the humanin peptide was analysed by western blotting and immunohistochemistry. Electron microscopic immunohistochemistry was performed to investigate the distribution of this peptide within the cell.
Results: 68 highly expressed genes were identified in PVNS. Humanin genes were strongly expressed in diffuse-type PVNS, but were barely detected in nodular-type PVNS, rheumatoid arthritis, or osteoarthritis. Humanin peptide was identified in synovium from diffuse-type PVNS, and most of the positive cells were distributed in the deep layer of the synovial tissue. Double staining with anti-humanin and anti-heat shock protein 60 showed that humanin was expressed mainly in mitochondria. Electron microscopy disclosed immunolocalisation of this peptide, predominantly around dense iron deposits within the siderosome.
Conclusions: Increased expression of the humanin peptide in mitochondria and siderosomes is characteristic of synovial cells from diffuse-type PVNS. Humanin is an anti-apoptotic peptide which is encoded in the mitochondrial genome. Present findings suggest that mitochondrial dysfunction may be the principal factor in pathogenesis of diffuse-type PVNS and that humanin peptide may play a part in the neoplastic process in this form of PVNS.

Pigmented villonodular synovitis (PVNS) is classified as an uncommon idiopathic proliferative synovial process.[1 2] It can exist in a localised form within a joint but more commonly occurs as a diffuse form where the entire synovium of a joint is affected.[3–7] The exact aetiology of PVNS is still unknown.[8–10] Previous experimental and epidemiological studies have suggested that PVNS is a reactive process involving a chronic inflammatory response.[11 12] However, recent studies showing the capacity of these lesions for autonomous growth and the potential for recurrence have suggested involvement of a neoplastic process.[13] The neoplastic hypothesis has been further supported by studies suggesting that heterogeneous proliferating cells, such as fibroblasts, histiocytes, multinuclear cells, and chronic inflammatory cells, might be neoplastic, with other cell types being reactive in nature.[14 15]

Histologically, PVNS is composed of proliferating mononuclear cells, with frequent giant cells, and intracellular and extracellular iron deposits. These iron deposits are observed as membrane bound particles in siderosomes. Interestingly, Schumacher *et al* and Ghadially *et al* reported that the siderosome fuses with mitochondria in deep synovial cells from patients with PVNS.[16 17] Moreover, abundant mitochondria throughout the cytoplasm were observed in dispersed stromal cells containing electron dense inclusions and in giant cells.[16 18]

In this study we searched for highly expressed genes in primary synovial cells from patients with PVNS compared with those from patients with rheumatoid arthritis (RA). We considered that a comparison of synovial cells from PVNS with those from RA, which are composed of chronic inflammatory cells, would identify the distinct nature of PVNS and define this proliferative process more precisely. Ribosomal RNA (rRNA) with poly A tail encoded by mitochondrial genes was highly expressed in PVNS. Among these genes, humanin has been reported to act as an oncopeptide or as an anti-apoptotic factor against Bax (Bcl2 associated X protein), which is an apoptosis-inducing protein.[19 20] However, little is known about the pathological role of humanin in diseases other than Alzheimer's disease.

We report here that the expression of humanin peptide is increased strongly in diffuse-type PVNS compared with other arthritides and it is abundant in mitochondria and siderosomes of synovial cells from PVNS.

METHODS

Synovial tissue preparation and RNA extraction

Synovial biopsy specimens were obtained during surgery from six patients with PVNS, three with RA, and three with osteoarthritis (OA). These lesions were subtyped into two types (diffuse or nodular) according to locations (intra-articular versus extra-articular) and pathological growth patterns, which reflected clinical characteristics and biological behaviour.[13]

Abbreviations: BSA, bovine serum albumin; GAPDH, glyceraldehyde-3-phosphate dehydrogenase; hsp, heat shock protein; IMDM, Iscove modified Dulbecco's medium; OA, osteoarthritis; PBS, phosphate buffered saline; PCR, polymerase chain reaction; PVNS, pigmented villonodular synovitis; RA, rheumatoid arthritis; RT-PCR, reverse transcriptase-polymerase chain reaction; SDS, sodium dodecyl sulphate; SDS-PAGE, sodium dodecyl sulphate-polyacrylamide gel electrophoresis; SSC, saline sodium citrate

The patients with RA met the criteria of the 1987 American College of Rheumatology. The tissue was cultured in Iscove modified Dulbecco's medium (IMDM) with collagenase V (1 mg/ml medium) for 40 minutes and cells were harvested through mesh and gathered by centrifugation. Total cellular RNA was extracted using acid-guanidinium-phenol-chloroform (AGPC) methods.[21] Equal aliquots were then electrophoresed on 1% agarose gels stained with ethidium bromide to compare large and small rRNA qualitatively and to exclude degradation. Poly A^+ RNA was purified from total RNA using the First Track kit (Invitrogen).

Double stranded cDNA synthesis and subtraction cloning

One microgram of total RNA sample was used to synthesise full length, double stranded cDNA using a SMART polymerase chain reaction (PCR) cDNA synthesis kit (Clontech). Subtraction cloning was performed with a PCR-Select cDNA subtraction kit (Clontech). Equal amounts of double stranded cDNAs from two patients with PVNS (diffuse type/lane 1, nodular type/lane 2 in fig 2) were used as tester cDNAs, and equal amounts of double stranded cDNAs from three patients with RA were used as driver cDNAs. PCR using CD163 primers was performed to estimate the efficiency of subtraction, and the expected decrease in CD163 in the subtracted sample was observed (data not shown).

Southern colony hybridisation

Subtracted cDNAs were ligated to TOPO vector (Invitrogen) and transformed into DH10B cells (Invitrogen) by electroporation. After blue-white selection with X-gal containing Luria-Bertani (LB) plates, white colonies were cultured overnight with 150 µl LB medium in sterile 1.5 ml tubes and centrifuged for 2 minutes at 12 000 g, and the pellet was resuspended in 10 µl LB medium. The medium was mixed completely and 2 µl was dotted onto a nylon membrane for Southern hybridisation. SMART double stranded cDNA was labelled with [^{32}P]dCTP by random priming (Stratagene). Membranes were hybridised in aqueous solution (5 × saline sodium citrate (SSC), Denhardt's solution, 0.1% sodium dodecyl sulphate (SDS), 10 mg salmon sperm DNA) overnight at 65°C. After washing at 65°C for 1 hour in 0.1 × SSC, 0.1% SDS, the membranes were exposed to *x* ray film (Eastman Kodak Co) with an intensifying screen at −80°C. Measurement of cDNA was performed by scanning with a BASS 1000 Densitometer (Fuji film), and normalisation against glyceraldehyde-3-phosphate dehydrogenase (GAPDH) cDNA hybridised subsequently on the same blots.

Table 1 Highly expressed genes in PVNS compared with RA

Genes	No
Mitochondrial	
16S rRNA	30
12S rRNA	5
Homosapiens tomoregulin mRNA	2
Homosapiens ARFGAP 1 protein mRNA	1
Mitochondrial proteolipid 68 MP homology	1
Inflammation	
β_2-Microglobulin mRNA	4
Transforming growth factor-β mRNA	1
Fibrogenolysis	
Arg/serpin 1 plasminogen activator-inhibitor 2 mRNA	1
Homosapiens similar to serine proteinase mRNA	1
Homosapiens similar to serine/arginine repetitive matrix mRNA	1
Iron metabolism	
Ferritin light chain mRNA	13
Cartilage degradation	
Homosapiens dihydropyrimidinase mRNA	1
Homosapiens osteopontin mRNA	1
Neoplastic	
L-Plastin mRNA	1
Others	
Eukaryotic translation elongation factor mRNA	2
Homosapiens Nef-associated factor mRNA	1
Unknown	2
Total	68 clones

DNA sequencing

Sixty eight cDNAs from differentially expressed clones were amplified with M13 reverse (5'-CAGGAAACAGCTATGAC-3') primers using thermal cycling conditions (96°C for 30 seconds, 50°C for 15 seconds, 60°C for 4 minutes for 25 cycles). The cDNAs were purified and sequenced using the ABI PRISM dye terminator cycle sequencing ready reaction kit with template suppression reagent (ABI PRISM). DNA sequences were analysed using DNASIS software and compared with sequences in GeneBank (National Center for Biotechnology Information, Bethesda, MD).

Northern hybridisation

Poly A^+ RNA (168 ng) samples of the synovium from five patients with PVNS, three with RA, and three with OA patients were loaded and fractionated through 1.0% agarose gels and transferred to Hybond-N+ nylon transfer membrane (Amersham). Purified human cDNA (40 ng) was labelled with [^{32}P]dCTP by random priming and applied to the membrane for hybridisation in aqueous solution (5 × SCC, Denhardt's solution, 0.1% SDS, 10 mg salmon sperm DNA, 50% formamide) overnight at 42°C. After washing at 42°C for 1 hour in 0.1 x SSC, 0.1% SDS, the membranes were exposed to *x* ray film (Eastman Kodak Co) with an intensifying screen at −80°C.

Semiquantitative reverse transcriptase-polymerase chain reaction (RT-PCR)

Total RNA (2.5 µg) from five patients with PVNS, three with RA, and two with OA was used for cDNA synthesis with oligo$(dT)_{12-18}$ as template primer using M-MuLV reverse transcriptase. The reaction was conducted in a final volume of 50 µl containing 1 ml of the transcribed cDNA probe, 200 µmol/l of each dNTP, 1 × PCR buffer including 1.5 mM $MgCl_2$ (Takara Biomedical), 0.4 µM forward and reverse primers, and 2.5 U Taq polymerase (Takara). All amplimers were amplified simultaneously with GAPDH as internal standard. The respective primer pairs were for cytochrome *c* (forward: 5'-GCATAAACAACATAAGCTTCTGA-3', reverse: 5'-CAGCAGATCATTTCATATTGCTT-3'), for ATPase (forward: 5'-TCTCATCAACAACCGACTAATCA-3', reverse: 5'-GATAAGTGTAGAGGGAAGGTTAA-3'), for NADH dehydrogenase (forward: 5'-TTTACTCAATCCTCTGATCAGGG-3', reverse: 5'-CGAATTCATAAGAACAGGGAGGT-3'), and for cytochrome *b* (forward: 5'-AATTACAAACTTACTATCCGCCA-3', reverse: 5'-TGGGCGAAATATTATGCTTTGTT-3'). The reaction mixtures were incubated for 3 minutes at 94°C, followed by 32 cycles of denaturation for 1 minute at 94°C, annealing for 1.5 minutes at 52°C, and extension for 1 minute at 72°C.

Cell and tissue processing for light microscopy and immunohistochemistry

To isolate synovial cells, the deep layers of synovium from diffuse-type PVNS were cultured in IMDM with collagenase

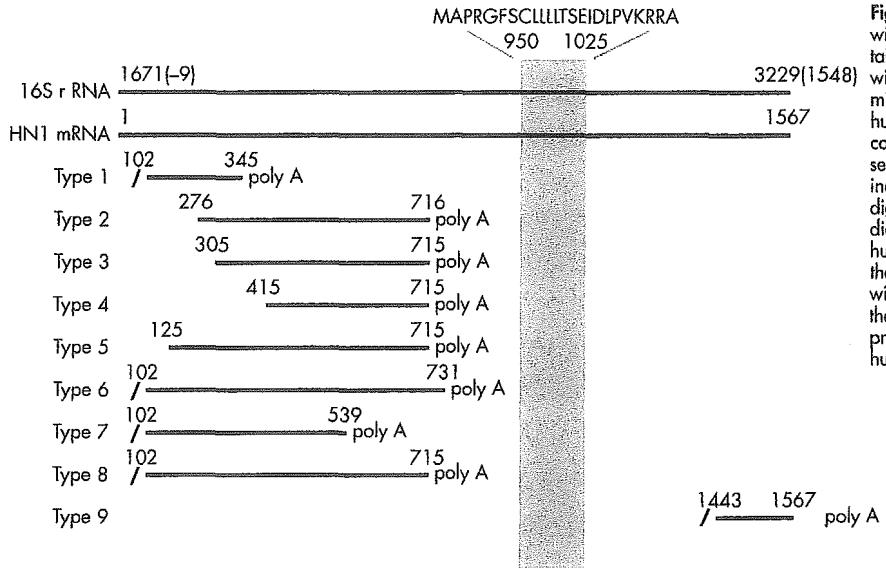

Figure 1 The sequences encoded within the 16S rRNA region with poly A tail. The cDNA fragments were aligned with the 16S rRNA region of the mitochondrial gene and the correlating humanin mRNA sequence. Southern colony hybridisations repeated these sequences in a total of three rounds independently. Oblique bars show the digestion sites by Rsa I and upward diagonal bar shows the region of humanin coding sequences. Although there are nine types of sequences with poly A tail within this region, only the type 9 sequence was identical to the previously reported mRNA encoding humanin peptide.

V (1 mg/ml medium) for 20 minutes and cells were harvested through mesh and gathered by centrifugation. These synovial cells were cultured in IMDM with 10% fetal bovine saline for 4 hours and fixed with 10% buffered formaldehyde at room temperature for 10 minutes, then rinsed with phosphate buffered saline (PBS). Formalin fixed tissue sections were also used for immunostaining. A rabbit polyclonal anti-humanin antibody was synthesised and purified on an affinity column and dissolved in PBS (0.9% NaCl, 0.02 M phosphate buffer, pH 7.0). The IgG concentration was analysed using a protein assay kit (Bio-Rad). Immunostaining was performed as previously described.[22 23] Briefly, cells and sections were fixed with 4% formaldehyde in PBS. After rinsing with PBS, membrane perforation treatment was performed with 95% ethanol/5% acetic acid for 10 minutes. After washing with PBS and blocking by incubation with 1% bovine serum albumin (BSA), excess BSA was then removed and the cells were incubated with anti-humanin antibodies overnight at 4°C. After rinsing, Alexa Fluor 488 goat antirabbit IgG (Molecular Probes Inc) was applied as a secondary antibody for 60 minutes. Immunofluorescence was detected with a CSU-10 confocal laser scanning unit (Yokogawa Electric Co), coupled to an IX90 inverted microscope with UPlanAPOX20 objective lens (Olympus Potical Co), and C5810-01 colour chilled 3CCD camera (Hamamatsu Photonics, KK). For double staining, anti-humanin antibody and anti-heat shock protein (hsp) 60 antibody (Santa Cruz Biochemistry Inc) were used as first antibodies, while Alexa Fluor 568 goat antirabbit IgG and Alexa Fluor 488 donkey antigoat IgG (Molecular Probes Inc) were used as a second antibodies.

Western blot analysis

Tissues were homogenised and lysed in a buffer consisting of 150 mM NaCl, 50 mM Tris HCl, pH 7.5, 0.5% Nonidet 40, 50 mM NaF, 1 mM Na_3VO_4, 1 mM phenylmethylsulphonyl fluoride, and 1% aprotinin at 4°C for 30 minutes. Cell lysates were cleared of cell debris by centrifugation at 14 000 *g* for 30 minutes. Protein (20 µg) was subjected to sodium dodecyl sulphate-polyacrylamide gel electrophoresis (SDS-PAGE) on

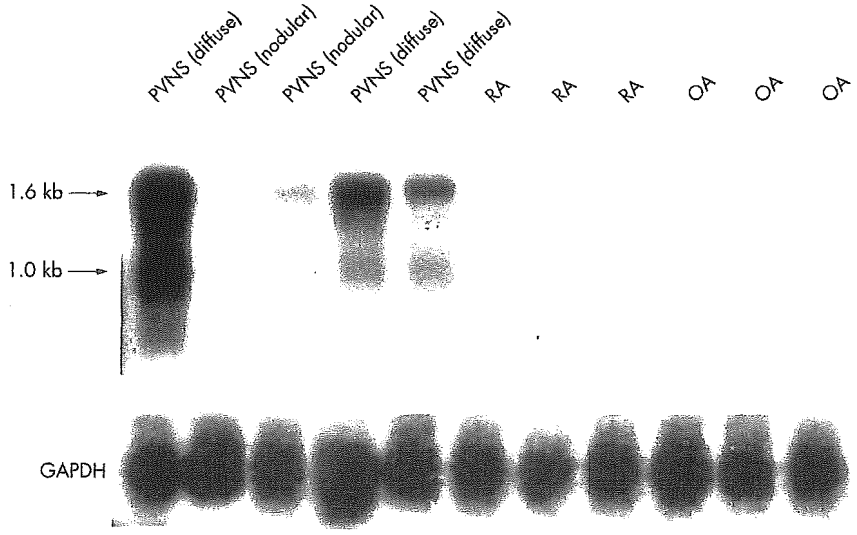

Figure 2 Northern blot analysis of mRNAs expressed by synovial cells from patients with PVNS, RA, and OA. Total RNA (168 ng) was subjected to electrophoresis in a 1.0% agarose gel containing formaldehyde, transferred to a nylon membrane, and probed with [^{32}P]dCTP labelled cDNA (type 9; fig 1). Another cDNA (type 3) encoded in the 16S rRNA region was also used in northern blotting and the expression level and size were same as those using type 9 cDNA (data not shown). Humanin genes were strongly expressed in diffuse-type PVNS, but barely detected in nodular-type PVNS, RA, or OA. The size of the expressed major message was ~1.6 kb and the other messages were ~1 kb, which corresponds to the results of a previous report by Hashimoto *et al*.[28]

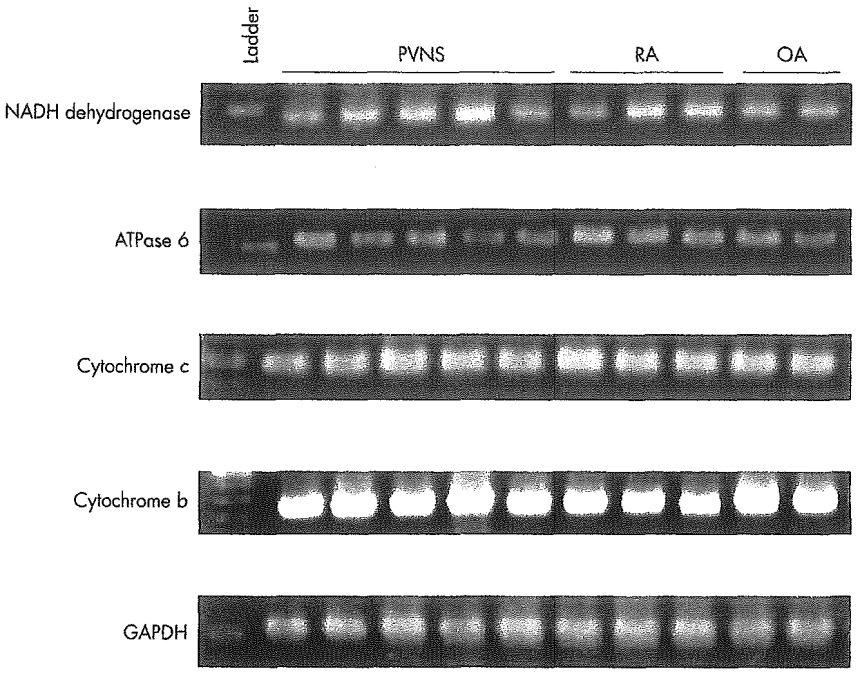

Figure 3 The expression of genes encoded in mitochondria other than humanin genes. Total RNA was extracted from the synovial cells of five patients with PVNS, three with RA, and three with OA, and NADH dehydrogenase, ATPase 6, cytochrome *c*, cytochrome *b*, and GAPDH mRNA levels were analysed by semiquantitative RT-PCR. The levels of expression of these genes in PVNS were not increased in other types of arthritis, indicating that the humanin gene was selectively expressed in mitochondrial genes in PVNS.

a PAG mini Daiichi 15/25 gel (Daiichi Pure Chemical Co). The gel electrophoresis was performed under non-reducing conditions. The proteins were then blotted onto a nitrocellulose blotting membrane (Osmonics Inc). Nitrocellulose membranes were blocked with 5% BSA, followed by washing with PBS-Tween 20, and incubated with rabbit anti-humanin antibody at 4℃ overnight. After intensive washing, membranes were incubated with horseradish peroxidase linked goat antirabbit IgG, followed by detection with enhanced chemiluminescence reagents (Biotechs).

Electron microscope and colloidal gold immunocytochemistry

Synovial cells from diffuse-type PVNS were gathered in the same manner for light microscopy, and fixed in 3% glutaraldehyde in 0.1 M phosphate buffer (pH 7.4) at 4℃ over night. The specimens were postfixed in 1% OsO_4 in 0.1 M phosphate buffer (pH 7.4) overnight at 4℃, rinsed three times (10 minutes each) in 10% saccharose, and stained all together in 3% aqueous uranyl acetate for 1 hour at room temperature. Samples were then dehydrated in an ascending series of ethanol concentrations, replaced by propylene oxide, and embedded in epoxy resin. Ultrathin sections (100 nm) were cut, stained with uranyl acetate and lead citrate, and observed using an electron microscope (Hitachi H-7000).

For electron microscopic immunocytochemistry, cells were fixed in 0.2% glutaraldehyde and 4% paraformaldehyde mixture in 0.1 M phosphate buffer (pH 7.4) at 4℃ overnight. The samples were embedded into Lowicryl K4M, and ultrathin sections (100 nm) were used for incubation with anti-humanin antibody overnight. Incubation with the biotinylated secondary antibody was performed at room temperature for 1 hour, and after washing with PBS and distilled water, incubation with colloidal gold streptavidin was performed for 1 hour. The sections were rinsed and dried, then stained with uranyl acetate and lead citrate, and electron microscopy was performed as described above.

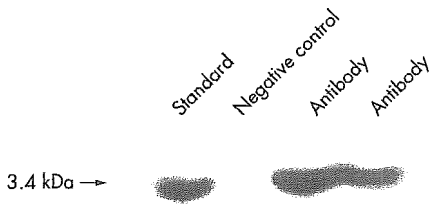

Figure 4 Expression of humanin peptide in synovial cells from diffuse-type PVNS. Protein (20 μg) from synovial cell lysates was subjected to SDS-PAGE on a 5–20% gradient gel. Rabbit anti-humanin polyclonal antibody was used for western blotting. Synthesised peptide, which was used as antigen to produce rabbit anti-humanin polyclonal antibody, was used as a standard and rabbit IgG was used as a negative control.

RESULTS

Identification of highly expressed genes in PVNS

A total of 2956 clones selected by subtraction cloning were further examined by Southern colony hybridisation. The sequencing was performed on genes expressed in PVNS at three times greater frequency than those in RA. Sixty eight of the highly expressed genes were identical to 17 known genes. Two genes were identical to genes encoding two hypothetical proteins. Table 1 classifies these genes into seven groups according to their functions and whether they were transcribed in mitochondria. Interestingly, genes encoded in the region of 16S rRNA and 12S rRNA were expressed with high frequencies. Furthermore, we detected various forms of 16S rRNA with poly A tail end, as shown in fig 1. No 12S rRNA with poly A tail was found among these genes. The cDNA with poly A tail (16S rRNA•3229: type 9 in fig 1) was identical to the humanin gene.

Northern blot analysis was performed using mRNA of synovial cells from patients with PVNS, RA, and OA. Humanin genes were strongly expressed in diffuse-type PVNS, but were barely detectable in nodular-type PVNS, RA, or OA (fig 2). However, other genes encoded by mitochondria were not increased as assessed by semiquantitative RT-PCR, suggesting

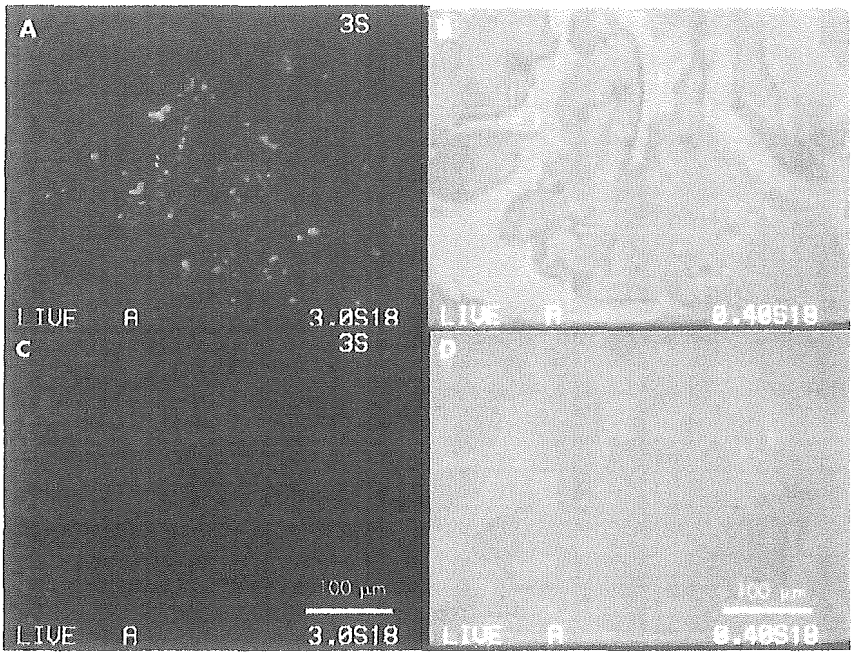

Figure 5 Synovial tissue from diffuse-type PVNS was fixed with 4% formaldehyde in PBS. The specimens were stained with anti-humanin antibody, followed by Alexa 488 goat antirabbit IgG, and photographed with a fluorescent microscope (×40). (A) Most positive cells (green) were distributed in a deep layer with haemosiderin deposit. (C) Negative control of the continuous section. (B, D) Backgrounds for (A) or (C), respectively.

that ribosomal genes were selectively expressed in mitochondrial genes in PVNS (fig 3). As far as we know, this is the first report of the expression of the humanin gene in synovial cells.

Expression of the humanin peptide in PVNS

Next, the expression of humanin peptide was identified using synovial cell lysates from diffuse-type PVNS and anti-humanin polyclonal antibody (fig 4). Immunohistochemical analysis showed that most of the positive cells were distributed in the deep layer (fig 5). This positive staining was thoroughly suppressed by blocking the primary antibody with synthesised antigen peptide (data not shown).

Although it has been suggested that the humanin peptide is expressed by cells in the deep layer of PVNS, little is known about the intracellular localisation of this peptide. In further examinations, we detected intracellular humanin peptide in synovial cells from diffuse-type PVNS. The humanin peptide was stained with a red colour, which localised in the cytoplasm of the synovial cells (fig 6B) but not in the nucleus. Mitochondria were stained with a green colour using anti-hsp60, which is mitochondrial-specific chaperonin (fig 6C). Double staining with anti-humanin antibody and anti-hsp60 (yellow colour) demonstrated that humanin was expressed mainly in the mitochondria (fig 6D).

Electron microscopic observation of synovial cells from diffuse-type PVNS showed that most of the iron deposits were included within the siderosome as described previously.[16 17] However, some electron dense iron deposits were

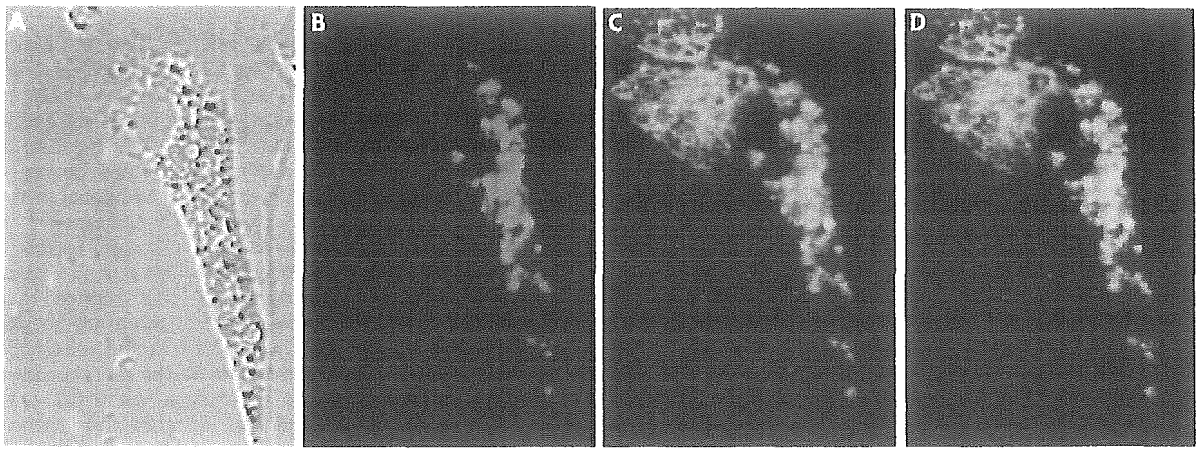

Figure 6 Relationship between humanin peptide expression and mitochondria. Isolated synovial cells containing haemosiderin were double stained with anti-humanin antibody and anti hsp60 antibody as first antibodies, followed by goat antirabbit IgG and donkey antigoat IgG as second antibodies (×400). (A) Haemosiderin was deposited unequally throughout the cytoplasm. (B) Single anti-humanin antibody staining (red). (C) Single anti-hsp60 antibody staining (mitochondrial staining; green). (D) Humanin was dominantly distributed in the mitochondria around the siderosome (yellow).

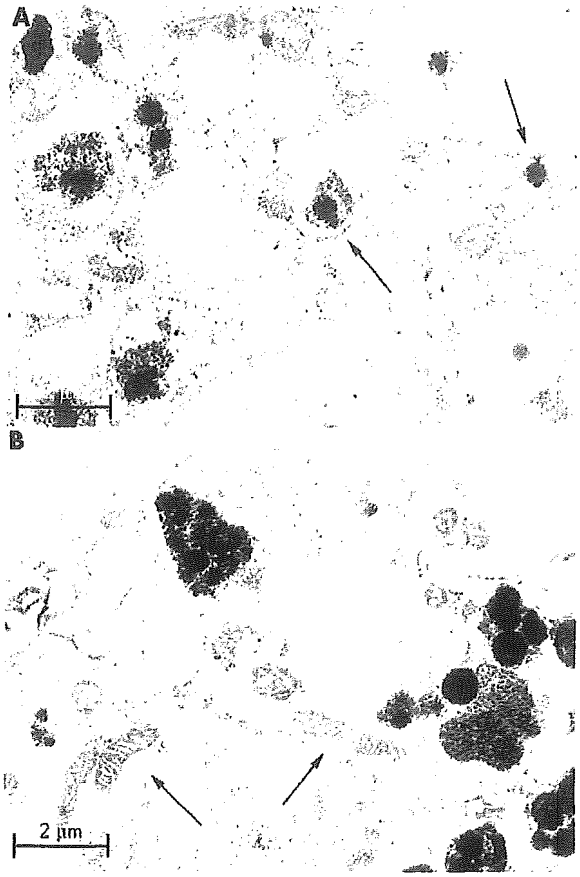

Figure 7 Electron micrograph of synovial cells from diffuse-type PVNS. Most of the electron dense iron deposits were observed within the siderosomes. Some electron dense iron deposits were observed within mitochondria (arrows). (A) Mitochondrial membrane debris with electron dense deposits was observed within the siderosome as an autophagosome (left arrow). (B) Some of the normal mitochondria (arrows) also were scattered throughout the cytoplasm. (Magnification ×19 000.)

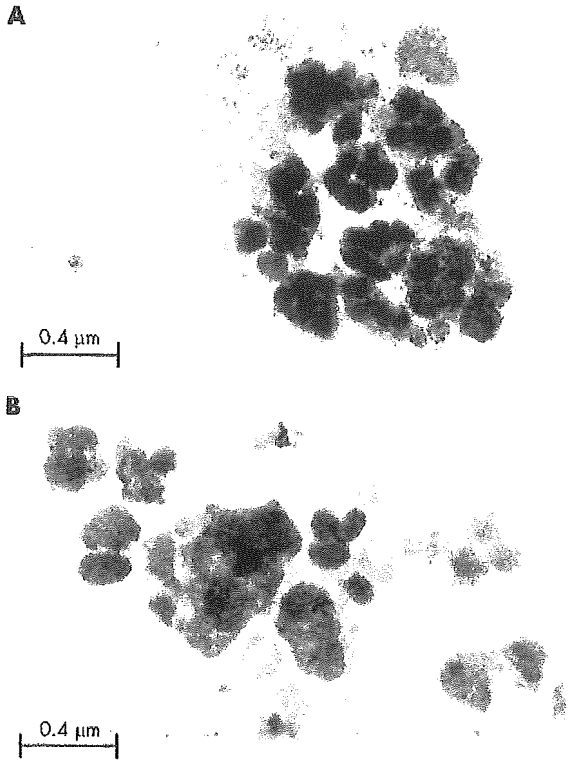

Figure 8 Electron microscopic immunohistochemistry of synovial cells from diffuse-type PVNS. (A) In some of the siderosomes, particles of colloidal gold, were precipitated in the debris adjacent to electron dense iron. These results demonstrate that humanin peptide is present within the debris that is phagocytosed into the siderosome. (B) Negative control for immunohistochemistry. (Magnification ×29 000.)

observed within the mitochondria (fig 7A). Interestingly, mitochondrial membrane debris with electron dense iron deposits were observed within the siderosome, which was characterised as an autophagosome (fig 7A). On the other hand, some normal mitochondria were scattered throughout the cytoplasm (fig 7B). Electron dense iron deposits within the siderosome were observed by electron microscopic immunohistochemistry (fig 8). In some siderosomes, particles of colloidal gold were precipitated in the debris adjacent to electron dense iron (fig 8A). These results suggest that humanin exists in mitochondria not only in the cytoplasm but also in the siderosome after being phagocytosed.

DISCUSSION

Genes with enhanced expression in synovial cells from PVNS were grouped according to their functions and the transcription in mitochondria as listed in table 1. It is likely that many of the listed genes play a part in the pathogenesis of PVNS according to their characterised functions. Interestingly, genes encoded in the regions of 16S rRNA and 12S rRNA were expressed with high frequencies. Previous reports pointed out the presence of polyadenylated transcripts of the 16S rRNA gene that differed from the 16S rRNA.[24–26] These poly A sequences are considered to be due to active metabolism of mitochondria in cancer cells, because the increased expression of the 16S rRNA genes was found only in malignancies.[19 27] These facts suggest that the genes encoded in the region of rRNA from PVNS reflect the neoplastic nature of this disease. In fact, for PVNS, especially the diffuse type, the neoplastic hypothesis is supported by the demonstration of aneuploid DNA content and the existence of cytogenetic aberration, as well as the capacity of these lesions for autonomous growth and the potential for recurrence.[13 14]

It is intriguing to examine whether these mitochondrial genes for 16S rRNA are virtually translated and act as functional peptides. In this regard, humanin is a polypeptide described as a rescue factor abolishing neural cell apoptosis. This peptide protects neural cells of the F11 line from death induced by the expression of mutated genes, causing early onset familiar Alzheimer's disease.[28] Additionally, it was reported that humanin protects CN-procaspase-3 from amyloid precursor protein-induced cleavage, thereby preventing apoptosis.[29–31] More recently, Guo *et al* also described the anti-apoptotic mechanism of this peptide through interference with Bax activation.[20] In this study we proved that the humanin peptide, encoded in the mitochondrial genome, was selectively expressed in the mitochondria and within the siderosome in the diffuse-type PVNS synovial cells. It is well established that damaged and functionally disabled mitochondria may be autophagocytosed by lysosomes to prevent continuous oxidative damage, as shown in the degenerating mitochondria within the siderosome in our electron microscopic study.[32 33] This evidence suggests that humanin is translated in mitochondria, leading to survival of

this organelle under the condition of excessive iron deposition.

In fact, extreme iron deposition is one of the most characteristic pathological features in PVNS.[2 7 8] This deposit is derived from the breakdown of erythrocytes that are phagocytosed after repeated bleeding into the joint space.[16 34 35] Under the condition of iron excess, some of the iron is shunted into haemosiderin and stored in the cytoplasm.[36] It is well described that reactive oxygen species are generated by excessive iron-induced cell apoptosis, which is one important mechanism implicated in the mitochondrial death pathway.[36–40] This mechanism may involve the capacity of excessive iron deposits to stimulate lipid peroxidation, thereby disrupting lysosomal membranes and releasing tissue destructive hydrolytic enzymes.[41 42] In regard to PVNS, as shown in our subtraction cloning, the iron deposits are known to be associated with large quantities of ferritin. Nevertheless, homogeneous synovial cells with small, rounded siderosomes in the deep layer of synovium, which present predominantly in diffuse-type PVNS, were reported to have minimum tissue damage adjacent to the iron deposits.[43] Morris *et al* reported that electron dense iron deposits were associated with mitochondrial destruction in haemophilic synovitis but much less so in PVNS.[43] Several explanations were suggested for this lack of mitochondrial damage in previous reports, such as transitional function during inflammation, or the failure of the apoferritin response.[31 43] However, there were no facts to explain this pathology.

The alternative intriguing explanation about this pathogenesis of PVNS is that a mitochondrial abnormality exists primarily in PVNS which is independent of the precipitation of haemosiderin. In that case, the overload of iron deposits in the cytoplasm and mitochondria could induce free radicals. However, abnormal mitochondria would be responsible for supplying a key reactant, humanin, to prevent oxidative damage until they are autophagocytosed within the siderosome, resulting in cell survival. In accordance with this view, analysis of isolated cells has enabled us to describe here for the first time the feature of mitochondria containing haemosiderin, which were autophagocytosed and degenerating within the siderosome, in addition to many mitochondria without haemosiderin scattered around the cytoplasm.

Taken together, our findings lead us to a simple interpretation that the possible function of humanin located within the mitochondria in PVNS synovial cells may be to serve as a rescue factor from excessive iron damage and consequent organelle breakdown in the cytoplasm and cell death. However, Hashimoto *et al* have shown that cell death is only supported by the secreted humanin peptide,[29] and the function of the peptide located intracellularly is still unclear. Although future studies are required to investigate the function of humanin within the cytoplasm, our data suggest that humanin is involved in the iron depositing pathology of PVNS. In conclusion, our results suggest that the humanin peptide is highly expressed in the synovial cells from diffuse-type PVNS and may play a part in the pathology of PVNS.

ACKNOWLEDGEMENTS

We thank A Tsuchiya MD and S Tsuyama MD for their professional advice.

Authors' affiliations

K Ijiri, H Sakakima, Course of Physiotherapy, School of Health Science, Faculty of Medicine, Kagoshima University, Kagoshima, Japan
K Ijiri, M B Goldring, Beth Israel Deaconess Medical Center, New England Baptist Bone and Joint Institute, Boston, MA, USA
H Tsuruga, T Matsuyama, Immunology and Medical Zoology, Graduate School of Medicine, Kagoshima University, Kagoshima, Japan
N Taniguchi, K Shimoonoda, S Komiya, Department of Neuro-Musculoskeletal Disorder, Kagoshima University Graduate School of Medicine and Dentistry, Kagoshima University, Kagoshima, Japan
K Tomita, H J Majima, Department of Oncology, Kagoshima University Graduate School of Medicine and Dental Science, Kagoshima, Japan

REFERENCES

1 **Jaffe HL,** Lichtenstein L, Sutro CJ. Pigmented villonodular synivitis, bursitis and tenosynovitis. *Arch Pathol* 1941;**31**:731–65.
2 **Dorwart RH,** Genant HK, Johnston WH, Morris JM. Pigmented villonodular synovitis of synovial joints: clinical, pathologic, and radiologic features. *AJR Am J Roentgenol* 1984;**143**:877–85.
3 **Darling JM,** Glimcher LH, Shortkroff S, Albano B, Gravallese EM. Expression of metalloproteinases in pigmented villonodular synovitis. *Hum Pathol* 1994;**25**:825–30.
4 **Gehweiler JA,** Wilson JW. Diffuse biarticular pigmented villonodular synovitis. *Radiology* 1969;**93**:845–51.
5 **Crosby EM,** Inglis A, Bullough PG. Mulitple joint involvement with pigmented villonodular synovitis. *Radiology* 1977;**122**:671–2.
6 **Wagner ML,** Spjut HJ, Dutton RV, Glassman AL, Askew JB. Polyarticular pigmented villonudular synovitis. *AJR Am J Roentgenol* 1981;**136**:821–3.
7 **Byers PD,** Cotton RE, Deacon OW, Lowy M, Newman PH, Sissons HA, *et al.* The diagnosis and treatment of pigmented villonodular synovitis. *J Bone Joint Surg Br* 1968;**50**:290–305.
8 **Jozsa L.** Immunohistochemical characterization of pigmented villonodular synovitis. *Zentralbl Pathol* 1992;**138**:119–23.
9 **O'Connell JX,** Fanburg JC, Rosenberg AE. Giant cell tumor of tendon sheath and pigmented villonodular synovitis. Immunophenotype suggests a synovial cell origin. *Hum Pathol* 1995;**26**:771–5.
10 **Darling JM,** Goldring SR, Harada Y, Handel ML, Glowacki J, Gravallese EM. Multinuclear cells in pigmented villonodular synovitis and and giant cell tumor of tendon sheath express features of osteoclasts. *Am J Pathol* 1997;**150**:1383–92.
11 **Young JM,** Hudacek AG. Experimental production of pigmented villonodular synovitis in dogs. *Am J Pathol* 1954;**30**:799–811.
12 **Sigh R,** Grewal DS, Chakravarti RN. Experimental production of pigmented villonodular synovitis in the knee and ankle joints of rhesus monkey. *J Pathol* 1969;**98**:137–42.
13 **Somerhausen NSA,** Fletcher CDM. Diffuse-type giant cell tumor. Clinicopathologic and immunohistochemical analysis of 50 cases with extraarticular disease. *Am J Surg Pathol* 2000;**24**:479–92.
14 **Abdul-Karim FW,** El-Naggar AK, Joyce MJ, Makley JT, Carter JR. Diffuse and localized tenosynovial giant tumor and pigmented villonodular synovitis: a clinicopathological and flow cytometric DNA analysis. *Hum Pathol* 1992;**23**:729–35.
15 **Fletcher JA,** Henkle C, Atkins L, Rosenberg AE, Morton C. Trisomy 5 and trisomy 7 are nonrandom aberrations in pigmented villonodular synovitis: confirmation of trisomy 7 in uncultured cells. *Genes Chromosomes cancer* 1992;**4**:264–6.
16 **Schumacher HR,** Latke P, Athreya B, Rothfuss S. Pigmented villonodular synovitis: light and electron microscopic studies. *Semin Arthritis Rheum* 1982;**12**:32–43.
17 **Ghadially FN,** Lalonde J-M A, Dick CE. Ultrastructure of pigmented villonodular synovitis. *J Pathol* 1978;**127**:19–27.
18 **Wyllie JC.** Stromal cell reaction of pigmented villonodular synovitis: an electron microscopic study. *Arthritis Rheum* 1969;**12**:205–14.
19 **Maximov V,** Martynenko A, Hunsmann G, Tarantul V. Mitochondrial 16S rRNA gene encodes a functional peptide, a potential drug for Alzheimer's disease and target for cancer therapy. *Med Hypotheses* 2002;**59**:670–3.
20 **Guo B,** Zhai D, Cabezas E, Welsh K, Niourain S, Tatterthwait A, *et al.* Humanin peptide suppresses apoptosis by interfering with Bax activation. *Nature.* 2003;423: 456–61, Epub 4 May, 2003.
21 **Chomczynski P,** Sacchi N. Single-step method of RNA isolation by acid guanidinium thiocyanate-phenol-chlorform extraction. *Anal Biochem* 1987;**162**:156–9.
22 **Majima JH,** Oberley TD, Fukukawa K, Mattson MP, Yen HC, Szweda LI, *et al.* Prevention of mitochondrial injury by manganese superoxide dismutase reveals a primary mechanism for alkaline-induced cell death. *J Biol Chem* 1998;**273**:8217–24.
23 **Motoori S,** Majima HJ, Ebara M, Kato H, Hirai F, Kakinuma S, *et al.* Overexpression of mitochondrial manganese superoxide dismutase protects against radiation-induced cell death in the human hepatocellular carcinoma cell line, HLE. *Cancer Res* 2001;**61**:5382–8.
24 **Peng G,** Taylor JD, Tchen TT. Increased mitochondrial activites in pigmented (melanized) fish cells and nucleotide sequence of mitochondrial large rRNA. *Biochem Biophys Res Commun* 1992;**189**:445–9.
25 **Baserga SJ,** Linnenbach AJ, Malcolm S. Polyadenylation of a human mitochondrial ribosomal RNA transcript detected by molecular cloning. *Gene* 1985;**35**:305–12.
26 **Tarantul V,** Nikolaev A, Hannig H. Detection of abundantly transcribed genes and gene translocation in human immunodeficiency virus-associated non-Hodgkin's lymphoma. *Neoplasia* 2001;**3**:132–42.
27 **Penta J,** Johnson FM, Wachsman JT, Copeland WC. Mitochondrial DNA in human malignancy. *Mutat Res* 2001;**488**:119–33.
28 **Hashimoto Y,** Niikura T, Tajima H, Yasukawa T, Sudo H, Ito Y, *et al.* A rescue factor abolishing neural cell death by a wide spectrum of familial Alzheimer's disease. *Proc Natl Acad Sci USA* 2001;**98**:6336–41.

29 **Hashimoto Y**, Ito Y, Niikura T. Mechanism of neuroprotection by a novel rescue factor humanin from Swedish mutant amyloid precursor protein. *Biochem Biophy Res Commun* 2001;**283**:460–8.
30 **Yu W**, Sanders BG, Kline K. RRR-alpha-tocopheryl succinate-induced apoptosis of human breast cancer cells involved bax translocation to mitochondria. *Cancer Res* 2003;**63**:2483–91.
31 **Nakazawa Y**, Kamijo T, Koike K, Noda T. ARF tumor suppressor induces mitochondria-dependent apoptosis by modulation of mitochondrial Bcl-2 family proteins. *J Biol Chem*. 2003;278: 27888–95, Epub 9 May, 2003.
32 **Muirden KD**. The anemia of rheumatoid arthritis: the significance of iron deposits in the synovial membrane. *Aust Ann Med* 1970;**2**:97–104.
33 **Brunk UT**, Terman A. The mitochondrial-lysosomal axis theory of aging: accumulation of damaged mitochondria as a result of imperfect autophagocytosis. *Eur J Biochem* 2002;**269**:1996–2002.
34 **Morris CJ**, Wainwright AC, Steven MM. The nature of iron deposits in haemophilic synovitis – an immunohistochemical ultrastructural and x-ray microanalytical study. *Virchows Arch A Pathol Anat Histopathol* 1984;**404**:75–85.
35 **Docken WP**. Pigmented villonodular synovitis: a review with illustrative case reports. *Semin Arthritis Rheum* 1979;**9**:1–22.
36 **Wixom RL**, Prutkin L, Munro HN. Hemosiderin: nature, formation, and significance. *Intl Rev Exp Pathol* 1980;**22**:193–225.
37 **Chamberlain MA**, Petts V, Gollins E. Transport of intravenously injected ferritin across the guinea-pig synovium. *Ann Rheum Dis* 1972;**31**:493–9.
38 **McCord JM**, Roy RS. The pathophysiology of superoxide; roles in inflammation and ischaemia. *Can J Physiol Pharmacol* 1982;**60**:1346–52.
39 **Halliwell B**, Gutteridge JM. Oxygen toxicity, oxygen radicals, transition metals and disease. *Biochem J* 1984;**219**:1–4.
40 **Panduri V**, Weitzman SA, Chandel N, Kamp DW. The mitochondria-regulated death pathway mediates asbestos-induced alveolar epithelial cell apoptosis. *Am J Respir Cell Mol Biol* 2003;**28**:241–8.
41 **Gutteridge JM**, Halliwell B, Treffry A, Harrison PM, Blake DR. Effect of ferritin containing fractions with different iron loading on lipid peroxidation. *Biochem J* 1983;**209**:557–60.
42 **Crichton RR**. Interreaction between iron metabolism and oxygen activation. In: *Oxygen free radicals and tissue damage*. Amsterdam: Excerpta Medica, 1979:57–76.
43 **Morris CJ**, Blake DR, Wainwright AC, Steven MM. Relationship between iron deposits and tissue damage in the synovium: an ultrastructural study. *Ann Rheum Dis* 1986;**45**:21–6.

Circulation
JOURNAL OF THE AMERICAN HEART ASSOCIATION

American Heart Association.
Learn and Live.

Mechanism of Persistent Ischemic Mitral Regurgitation After Annuloplasty: Importance of Augmented Posterior Mitral Leaflet Tethering

Fang Zhu, Yutaka Otsuji, Goichi Yotsumoto, Toshinori Yuasa, Takayuki Ueno, Bo Yu, Chihaya Koriyama, Shuichi Hamasaki, Sadatoshi Biro, Akira Kisanuki, Shinichi Minagoe, Robert A. Levine, Ryuzo Sakata and Chuwa Tei

Circulation 2005;112;396-401
DOI: 10.1161/CIRCULATIONAHA.104.524561
Circulation is published by the American Heart Association. 7272 Greenville Avenue, Dallas, TX 72514
 Print ISSN: 0009-7322. Online ISSN: 1524-4539

Mechanism of Persistent Ischemic Mitral Regurgitation After Annuloplasty

Importance of Augmented Posterior Mitral Leaflet Tethering

Fang Zhu, MD*; Yutaka Otsuji, MD*; Goichi Yotsumoto, MD; Toshinori Yuasa, MD; Takayuki Ueno, MD; Bo Yu, MD; Chihaya Koriyama, MD; Shuichi Hamasaki, MD; Sadatoshi Biro, MD; Akira Kisanuki, MD; Shinichi Minagoe, MD; Robert A. Levine, MD; Ryuzo Sakata, MD; Chuwa Tei, MD

Background—We hypothesized that surgical annuloplasty for ischemic mitral regurgitation (MR) that displaces the posterior annulus anteriorly can potentially augment posterior leaflet (PML) tethering, leading to persistent MR. Relationships between leaflet configurations and persistent ischemic MR after the annuloplasty were investigated.

Methods and Results—In 31 patients with surgical annuloplasty for ischemic MR and 20 controls, posterior and apical displacement of the leaflet coaptation, the anterior leaflet (AML) and PML tethering angles relative to the line connecting annuli, coaptation length (CL), and the MR grade were quantified before and early after surgery in echocardiographic left ventricular long-axis views. Six of the 31 patients showed persistent MR despite annuloplasty. Compared with patients without persistent MR, those with MR showed no improvement in the left ventricular ejection fraction and systolic volume, similar reduction in the annular area, significant increase in posterior displacement of the coaptation ($P<0.01$), no improvement in AML tethering, greater worsening in PML tethering ($P<0.01$), and no increase in the CL. All tethering variables were significantly correlated with both preoperative and postoperative MR in univariate analysis, and reduced CL was the primary independent determinant of both preoperative and postoperative MR. Although increased AML tethering was the primary determinant of the preoperative CL ($r^2=0.46$, $P<0.0001$), increased PML tethering was the primary determinant afterward ($r^2=0.60$, $P<0.0001$).

Conclusion—Although tethering of both leaflets is the major determinant of ischemic MR before surgical annuloplasty, both leaflets tethering but with predominant and augmented PML tethering is related to persistent ischemic MR after the annnuloplasty. (***Circulation.* 2005;112[suppl I]:I-396–I-401.**)

Key Words: mitral valve ■ echocardiography ■ valuloplasty

Current surgical approaches for the treatment of ischemic mitral regurgitation (MR) mainly focus on annular size reduction, which is usually effective.[1–3] A considerable number of patients, however, show persistent or recurrent MR despite annuloplasty,[3–6] which adversely affects patients' outcomes,[7] and its mechanism has not been fully investigated.

The basic mechanism of ischemic MR is leaflet tethering by the outward displacement of papillary muscles (PM) due to left ventricular (LV) remodeling.[8–13] Surgical mitral annuloplasty, which is expected to hoist the posterior annulus anteriorly but may not cause significant positional changes to the anterior annulus fixed at the aortic root, can potentially augment tethering of the posterior mitral leaflet (PML) and restrict its anterior excursion toward coaptation while keeping the tethering of anterior leaflet (AML) unchanged (Figure 1).[6,14] We hypothesized that ischemic MR without annuloplasty is related to tethering of both leaflets and that MR after surgical annuloplasty is also related to tethering of both leaflets, but especially with tethering of the PML. Therefore, the purpose of this study was to investigate AML and PML configurations in patients with ischemic MR with and without surgical annuloplasty, and to clarify the characteristics of leaflet configurations responsible for persistent ischemic MR afterward.

Methods

Subjects

Subjects were 31 consecutive patients who had undergone surgical annuloplasty for ischemic MR at our hospital and 20 normal controls. Posterior annuloplasty with a flexible linear reducer (stain-

From the Department of Cardiovascular, Respiratory, and Metabolic Medicine (F.Z., Y.O., T.Y., B.Y., S.H., S.B., A.K., S.M., C.T.), Department of Public Health (C.K.), Department of Cardiovascular Surgery (G.Y., T.U., R.S.), Graduate School of Medicine, Kagoshima University, Kagoshima, Japan; and Massachusetts General Hospital (R.A.L.), Boston, Mass.

*The first 2 authors contributed equally to this work.

Correspondence to Yutaka Otsuji, MD, Department of Cardiovascular, Respiratory and Metabolic Medicine, Graduate School of Medicine, Kagoshima University, 8-35-1 Sakuragaoka, Kagoshima City, 890-8520, Japan. E-mail yutaka@m.kufm.kagoshima-u.ac.jp

Circulation **is available at http://www.circulationaha.org** **DOI: 10.1161/CIRCULATIONAHA.104.524561**

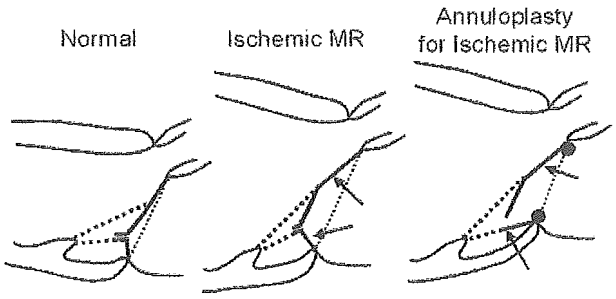

Figure 1. Potentially augmented tethering of the posterior mitral leaflet (PML) induced by surgical ring annuloplasty. The outward displacement of papillary muscles (PM) similarly tethers both anterior leaflet (AML) and PML with increased angles between the leaflets and the line connecting the mitral annuli (middle). Anteriorly hoisted posterior mitral annulus by ring annuloplasty may increase the distance between the PM tip and posterior annulus, thereby increasing tethering of the PML, with unchanged tethering of the AML (right).

less steel wire seemed with a polyester sheath), in addition to a Carpentier Edwards semi-rigid ring and a Duran flexible ring, was performed.[15] Patients profiles are summarized in Table 1. Ischemic MR was diagnosed by echocardiography using the following criteria: (1) The presence of LV dilatation and/or dysfunction, (2) the presence of apical displacement of mitral leaflets,[8] and (3) the absence of organic leaflet lesions. The control subjects had normal echocardiogram without known cardiovascular disease. After cardiovascular surgery with ring annuloplasty, no patient had a subsequent myocardial infarction or required additional revascularization. Concomitant coronary artery bypass grafting was performed in all patients and LV plasty with Dor's, overlapping of anterior wall,[16] or plication of posterior aneurysm was performed in 11 patients. Patients were managed after surgery with standard medications. Written informed consent was obtained from all patients.

Measurements by Echocardiography

Two-dimensional and Doppler echocardiographic examinations were performed in all patients using 2- to 3-MHz transducers and commercially available phased array sector scanners (ATL HDI 3000; Toshiba SSH 380A; Philips Medical Systems Sonos 5500; Aloka SSD-5500; Siemens Sequoia 512) 1 week before and 2 weeks to 2 months after the surgery.

LV end-diastolic volume, end-systolic volume (LVESV), and ejection fractions (EF) were determined by the modified biplane Simpson's method. The LV sphericity was assessed by its short-to-long axis dimension ratio in the end-systolic apical 4-chamber view. Mid-systolic mitral annular dimension was measured in the apical 4- and 2-chamber views, to calculate its area with an elliptical assumption.[17]

TABLE 1. Patient Profile

	All Subjects (n=31)	After Operation MR(+) (n=6)	After Operation MR(−) (n=25)	*P* value
Age	41 to 80 (63±12)	55 to 78 (69±8)	41 to 80 (62±12)	N.S.
Male/Female	25/6	5/1	20/5	N.S.
NYHA class	2 to 4 (3.0±1.0)	2 to 4 (3.0±1.0)	2 to 4 (3.0±1.0)	N.S.
Angina Pectoris	15	1	14	N.S.
Associated prior infero-posterior MI	11	2	9	N.S.
Prior anterior MI	13	1	12	N.S.
Prior anterior + infero-posterior MI	7	3	4	N.S.
Time lapse from first AMI, years	0.6 to 16 (7±6)	0.6 to 7 (5±3)	0.6 to 16 (7±7)	N.S.
Time lapse between surgery and post-operative echo, months	0.5 to 2.0 (1.0±0.5)	0.5 to 2.0 (1.0±0.5)	0.5 to 2.0 (1.0±0.5)	N.S.
Coronary risk factors				
Hypercholesterolemia	5	0	5	N.S.
DM	7	0	7	N.S.
Hypertension	9	1	8	N.S.
Smoking	10	2	8	N.S.
LV plasty	11	2	9	N.S.
Dor's	6	1	5	N.S.
Overlapping	4	0	4	N.S.
Plication of posterior aneurysm	1	1	0	N.S.
Number of CABG	1 to 5 (3.0±1.4)	1 to 3 (2.0±1.4)	1 to 5 (3.0±1.3)	N.S.
MV plasty				
Semi-rigid ring	12	2	10	N.S.
Carpentier Edwards ring size (mm)	26 to 32 (29±2)	26 to 32 (29±3)	26 to 32 (28±2)	N.S.
Flexible ring	19	4	15	N.S.
Duran ring (29 mm)	2	2	0	N.S.
Posterior annuloplasty with linear reducer	17	2	15	N.S.

NYHA indicates New York Heart Association; MI, myocardial infarction; AMI, acute myocardial infarction; DM, diabetes mellitus; LV, left ventricle; CABG, coronary artery bypass grafting; MV, mitral valve.

P values were obtained by χ^2 test.